Synthesis of Photocatalytic Membranes and Photocatalytic Membrane Reactors

Submitted by

Rahatun Akter

The EM3E4SW Master is an Education Programme supported by the European Commission, the European Membrane Society (EMS), the European Membrane House (EMH), and a large international network of industrial companies, research centres and universities

Synthesis of Photocatalytic Membranes and Photocatalytic Membrane Reactors

by

Rahatun Akter

Erasmus Mundus Masters in Membrane Engineering for a Sustainable World
(www.em3e.eu)

Submitted in Partial Fulfillment of the Requirements for the Degree of

Masters of Membrane Engineering, 2018-19

in the Department of Chemical Engineering and Environmental Technology

Faculty of Science, Universidad de Zaragoza

University de Montpellier

University of Chemistry and Technology, Prague

Under the Guidance of

Professor Dr. Reyes Mallada Viana

Department of Chemical Engineering and Environmental Technologies

Universidad de Zaragoza

Abstract

Fabrication of TiO_2 immobilized photocatalytic membranes (PMs) is a promising technique for advanced wastewater treatment applications. In this study, we fabricated TiO_2-based UV-sensitive PMs using two different methods. The first one was a TiO_2 coated Polyvinylidene fluoride (PVDF) membrane prepared using sol-gel synthesis method. Immersion of membrane in different concentrations (2 mM to 32 mM) of titanium isobutoxide (TIB), and ethanol solution, we deposited TiO_2 directly on the hydrophilic PVDF surface. Then, we used a low-temperature hydrothermal treatment to transform the in-situ synthesized TiO_2 to its most photoactive anatase phase. To prepare second PMs, TiO_2 blended PVDF membrane, we used electrospinning method to produce a mat of polymeric nanofibers. Our proposed method aimed to produce a highly porous membrane to have a higher surface area as well as enhance pollutant access to TiO_2. Using a bipolymer system, consists of polyvinylpyrrolidone (PVP) and PVDF, we immobilized P25-TiO_2 into a thin-film mat of highly porous electrospun nanofibers. Later removal of PVP by washing with water, we obtain highly porous electrospun nanomat. We used 70 ml of 6.4 mg/L Methylene Blue (MB) to assess the adsorption phenomena and visualize contaminant removal treated by membranes in a batch reactor. We fitted the adsorption kinetics data to a batch adsorption kinetic equation and photodegradation reaction kinetics to the Langmuir-Hinshelwood model. Among all TiO_2 coated PVDF membrane, PMs prepared from 16 mM sol-gel had the highest sorption (7.02 $\mu g/cm^2$ PMs) and degradation efficiency (98% in 4 h) with an apparent rate constant of 0.014 min^{-1}. On the other hand, highly porous electrospun TiO_2/PVDF nano-mat adsorbed a similar quantity of MB (7.03 $\mu g/cm^2$ PMs), and removed 100% MB after only 80 minutes of UV exposure and had an apparent kinetic constant of 0.094 min^{-1}. Therefore, the advantages of TiO_2/PVDF based highly porous electrospun nano-mat highlights the potential of applying this membrane in dye contaminated wastewater treatment.

Keywords: Photocatalytic Membranes, Photocatalytic Membrane Reactors, TiO_2, PVDF, Sol-gel synthesis, Electrospinning

Dedication

"DEDICATED TO

MY

BELOVED FAMILY MEMBERS"

FOR THEIR LOVE, ENDLESS SUPPORT,
ENCOURAGEMENT & SACRIFICES

Acknowledgements

I would like to take this opportunity to express my heartfelt gratitude to all those who have contributed me to make my thesis work possible through their help and support along the way. First and foremost, I would like to thank ALMIGHTY, who has provided me the strength to do justice to my work and contribute my best to it so that it has turned out to be a successful venue.

I express my sincere and wholehearted thanks, to my esteemed mentor **Dr. Reyes Mallada Viana**, Professor, Chemical Engineering and Environmental Technologies, Universidad de Zaragoza, Spain, for her regular inspiration, advice, the magnitude of dynamic and untiring guidance, and suggestion throughout the course of the present research. I am highly indebted to her relentless perseverance, which helped me to present this work in the right perspective, assuming the full form of the thesis. Throughout my works, she was like an angel and a constant source of inspiration. I really appreciate her support from the bottom of my heart. She spent countless hours of reflecting, reading, and encouraging throughout the entire process. Her outstanding guidance always encouraged my scientific thinking and instilled me with a sense of discipline in my work.

I express my heart full thanks to Dr. Nuria Navascues for her help and guidance with TGA, XRD testing, and organizing the chemicals and materials for this project testing. I would also like to thank to Dr. Marta Navarro Rojas, Dr. Gala Simón Ramírez, for their valuable guidance, technical and moral support during SEM analysis. My Special gratitude goes to Cristóbal Carrillo Pinzón for his cordial help throughout the lab work. Special thanks to all of the researchers in INA for their friendly assistance and advice in the lab.

I am very much thankful to my friend Shadi Alnahari, EM3E4SW student, session 2018-20, for helping me in preparing my membranes and giving me some of his previous samples and data that helped me a lot in designing the thesis work and report.

I would like to express my sincere thanks to EM3E4SW for giving me such an opportunity to pursue my study in such world-class institutions, use cutting edge lab facilities and acquire knowledge for my best future. I would like to acknowledge financial support from the European Union in the form of Erasmus mundus scholarship.

There are no words to express gratitude and thanks to my family members and friends for their immense support, and unfettered encouragement at all stages. I would like to thank each and every individual who has been a source of support and encouragement and helped me to achieve my goal and complete my dissertation work successfully.

Lastly, and most importantly, my overwhelming thanks goes to my husband, Md. Sadi Rahman, for his endless love without expecting any reward and providing his cooperation and mental support by standing with me to get through all the challenges experienced as an international student.

Rahatun Akter

June, 2020

Table of Contents

List of tables

List of Figures

1. Introduction

1.1 Photocatalysis for water treatment

Photocatalysis is a light-induced reaction, which is initiated by the presence of a photocatalyst. Photocatalysis requires a light source, which can be one of the cleanest and environmentally friendly forms of all energy sources, sunlight, but also fluorescent lamps [1], or Light Emitting Diodes (LED) [2] of different wavelenght. In the case of sunlight, this sustainable technology can be an ideal alternative for highly cost-sensitive or energy-restrictive situations [3].

When a beam of light with a specific wavelength irradiates the surface of a photocatalyst, it absorbs the photon energy and generates an electron-hole pair to form excited electrons. The generated electron reacts with O_2 to produce superoxide radical ion O^{2-}. At the same time holes interact with water molecules to form highly reactive oxygen species (ROS), such as hydroxyl radicals, $^{\circ}OH$, which consequently oxidize or reduce materials, or degrade organic pollutants from wastewater and generate harmless and low molecular weight products such as H_2, CO_2, and H_2O and so on [4]. The ROS can efficiently mineralize the wastewater contained organic pollutants, for instance, dyes (for example, methylene blue (MB), Reactive black (RB) etc.), pharmaceuticals, humic acids (HA), phenolic compounds, fulvic acids, synthetic organic matter, and natural organic matter etc. Hence this process can be used in water purification and wastewater treatment or decontamination applications.

Various semiconductor materials, for example, oxides (TiO_2, ZnO, CeO_2, ZrO_2, WO_3, V_2O_5, Fe_2O_3, etc.) and sulfides (CdS, ZnS, etc.) and their composites, for instance, Ag-AgI, Ag-TiO_2, g-C_3N_4, rGO/g-C_3N_4, CNTs/g-C_3N_4, CdS/g-C_3N_4 and Fe-$ZnIn_2S4$ have been used as photocatalysts [5]. Among them, TiO_2 is the most used photocatalyst in air purification, solar energy conversion, and wastewater treatment because of its lower cost, lower photo-erosion, less toxicity for health and environment, high thermal stability and chemical stability under UV irradiation [6]. Under UVA light, the anatase phase of titania, with a bandgap of 3.2 eV, can generate a high number of hydroxyl radicals than other phases of TiO_2. It shows the best photocatalytic performances with maximum quantum yields [5].

The TiO_2 can be used as a slurry of particles, especially as nanoparticles to have a high surface area as well as a mineralization rate. It is complicated to separate and reuse the nanoparticles from clear water after treatment, consequently a high risk of secondary pollution to occur. To

overcome the separation problem, researchers suggested two approaches to recover and reuse the TiO_2 nanoparticles efficiently; one is by employing coagulation and sedimentation [7], and another solution is membrane filtration [6]. However, both approaches required extra units to separate and recycle the nanoparticles, which are not only time consuming but also related to high cost and volume. Also, in a typical slurry reactor, the intensity of incident light can be altered due to the light scattering by dense colloidal slurry [3] and resulting in the low photo-conversion efficiency. These are the major gaps between the small-scale laboratory work and large scale applications of photocatalysis [8] [9].

1.2 Photocatalytic membranes (PMs)

The photocatalytic membrane provides an appealing solution towards the time-consuming, high processing water volume, and cost-related nanoparticle separation problems. The photocatalytic membrane integrates photocatalysis and membrane filtration steps into a single unit [6]. TiO_2 based PMs can be prepared by embedding a layer of TiO_2 nanoparticles on a membrane or blending it with membrane materials. Ideally, substrate materials should provide a strong bonding with TiO_2 to prevent catalyst leaching, stability against UV irradiation, and selective affinity to organic pollutants [10]. Alumina, zeolite, glass, ceramic, silica, and activated carbon, etc. are the commonly used inorganic substrate materials [11]. Past studies used inorganic membranes as a support material to coat TiO_2 while recently polymeric membranes have attracted many studies in the preparation of PMs. The easy and comparatively low cost in manufacturing processes, flexibility in membrane structures, and crack-free thin membranes in large scale productions are the main reasons for polymeric membranes to be selected over the inorganic membranes. In case of polymer-based supports, polyvinylidene fluoride (PVDF), polyethersulfone (PES), polysulfone (PS), polypropylene (PP), polyethylene (PE), polyacrylonitrile (PAN), polytetrafluoroethylene (PTFE), Polyvinyl chloride (PVC), cellulose acetate (CA) and Nafion, etc. are mainly used in PM applications [6] [11][12].

PVDF is a commonly used polymer in wastewater treatment and food applications because of its high strength and nontoxicity [13]. Besides, high chemical and UV stability [5] are the main reason for using in PM field. However, its high hydrophobicity is the key issue preventing the use of PVDF membranes in wastewater treatment applications. Incorporating the TiO_2 nanoparticles into PVDF membranes can solve this problem because the hydroxyl groups of TiO_2 would improve membrane hydrophilicity [13][14]. TiO_2 based PVDF photocatalytic membranes can be prepared

by depositing a layer of TiO_2 nanoparticles on the PVDF membrane surface[14]–[19] or by blending TiO_2 nanoparticles with PVDF matrix (mixed matrix membranes, MMMs) [2] [19]–[25]. The membrane performances, such as photocatalytic efficiency, and membrane surface properties, for instance, antifouling property, are greatly influenced by the TiO_2 immobilization method [28]. Therefore, the preparation method of the TiO_2/PVDF membrane is an indispensable part of the photocatalytic membrane field.

1.2.1 TiO_2 coated PVDF membranes

TiO_2 nanoparticles can anchor on the PVDF surface directly from Evonik P25 suspension (Fig. 1) or in-situ synthesis from TiO_2 precursors, for example, titanium tetra-isopropoxide (TTIP), or titanium isobutoxide (TIB). In this case, the pre-fabricated hydrophobic PVDF membrane surfaces need functionalization by i.e. generating -COOH or -OH group on the membrane surface to anchor the TiO_2 nanoparticles. The functionalized surface strongly binds TiO_2 via ion coordination or hydrogen bonding on the membrane surface [16] or trapped TiO_2 nanoparticles in surface nano-valleys (Fig. 1) [20].

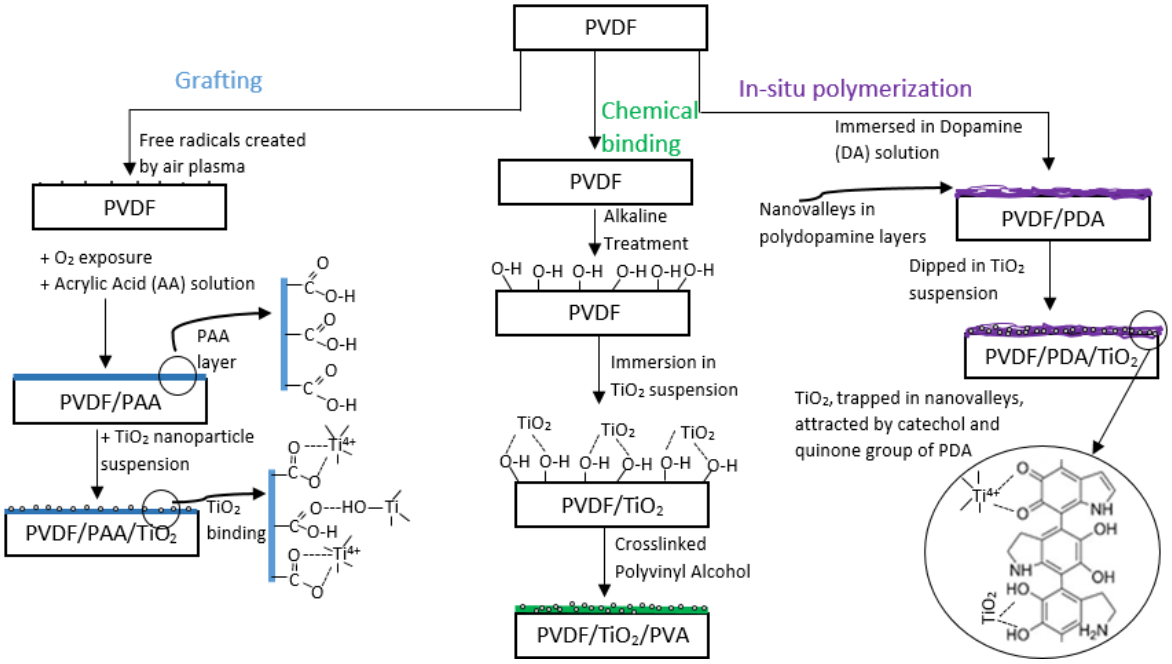

Fig. 1 PVDF surface functionalization and immobilization of TiO_2 nanoparticles on PVDF membrane surface

Grafting [17], chemical treatment [14][19], and in-situ polymerization [20] are the commonly used PVDF membrane surface functionalization method. Grafting incorporates a layer of hydrophilic polymer (polyacrylic acid) to provide -COOH groups on the PVDF membrane surface [17], while chemical binding yields OH group [14][19]. Besides, in-situ polymerization of

dopamine on membrane surface can generate nano-valleys from the relatively rough and loose structure of polydopamine to trap TiO_2 nanoparticles. Also, catechol and Quinone formed from polydopamine attract TiO_2 nanoparticles [20].

On the other hand, the sol-gel synthesis (Fig. 2) or chemical vapor deposition (CVD) are commonly used method for in-situ synthesis technique to anchor TiO_2 on PVDF membrane surface directly from its precursor. CVD technique [18] [29] used a Ti-target in the presence of a gaseous mixture of argon and oxygen to have in-situ nucleation and growth of TiO_2 nanoparticles onto PVDF porous membranes. The thickness and quality of obtained surface coatings depends on sputtering conditions [18] [29].

Sol-gel synthesis is a commonly used method to produce TiO_2 nanoparticles due to its simple operation, low reaction temperature, good chemical homogeneity, low requirements for the substrates, and high purity of the product [30]. The sol-gel solution can be prepared by adding a TiO_2 precursor (TTIP or TIB) into a solvent, for example, ethanol. Immersion of a wet hydrophilic PVDF membrane into a TTIP/ethanol solution provides TiO_2 coated surface by initiating hydrolysis reaction and growth of TiO_2 nanoparticles on the membrane (Fig. 2) [16]. J. Hou et al. [15] added 2,4-pentanedione as a chilling agent to stabilize the TTIP/ethanol sol-gel solution, perchloric acid ($HClO_4$) to have an acidic solution (pH ~1.2) and increase hydrolysis the reaction rate, and Milli-Q water to initiate the hydrolysis reaction. In this case, R-OH group of hydrophilic PVDF surface provides a strong and stable TiO_2 nano-layer by establishing R–O–Ti bonds during the gelation process [15], or via the connection of Ti^{4+} ion with two oxygen atoms of carboxylate (COOH) group or by forming hydrogen bonds between the carbonyl group and the surface hydroxyl group of TiO_2 [12].

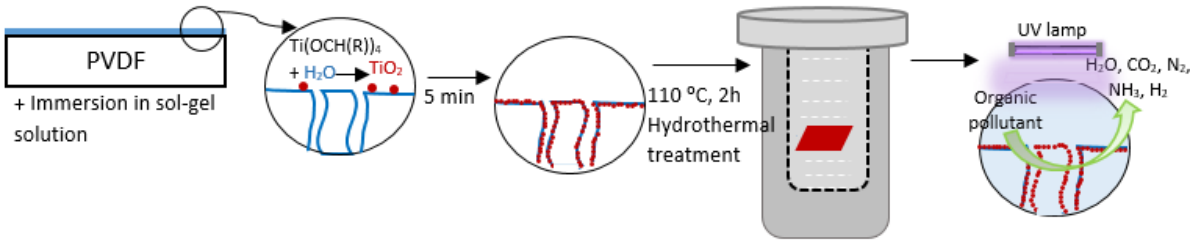

Fig. 2 Fabrication of TiO_2 nanoparticles coated PVDF membrane by sol-gel synthesis

However, sol-gel synthesis gives rise to amorphous TiO_2 nanoparticles [31][16] and a thermal treatment above 400 °C is needed to get the most photocatalytic-active stable anatase phase. The substrate materials PVDF membrane is sensitive to high temperatures. Therefore, a low-temperature hydrothermal treatment (LTHT), heating at 110 °C for 2 hours in the presence of water

as a catalyst, can be done to crystalize the TiO_2 [16]. Besides, LTHT yields a smooth membrane surface, which resists the deposition of fouling agents and improves the binding of TiO_2 with the membrane surface[16]. Table 1 shows a summary of the different preparation methods discussed above for TiO_2 coating on PVDF membranes, together with their advantages and disadvantages including some examples.

Table 1 UV sensitive TiO_2 coated PVDF membranes

Preparation Method	Supported membrane and used solution or precursor with solvent	Advantages	Disadvantages	Ref.
Sol-gel synthesis	Hydrophilic PVDF, TTIP, and ethanol	Hydrophilic PVDF provides formation of a stable and strong binding of TiO_2 layer with membrane surface, due to the R–O–Ti bond formed during the insitu gelation process (Fig. 2).	Sol-gel grown amorphous TiO_2 nanoparticles [16] need to be crystallized at low temperature due to high temperature-sensitive PVDF support.	[16]
	Hydrophilic PVDF, TTIP, ethanol, 2,4-pentanedione, $HClO_4$ and Milli-Q water			[15]
Chemical vapor deposition	PVDF, Ti-target in the presence of a gaseous mixture of argon and oxygen	Have in-situ nucleation and growth of TiO_2 nanoparticles onto PVDF porous membranes.	Series of time consuming experiments are necessary to find out the optimal set of parameters (sputtering power and time, target distance and gas pressure) for a homogeneous membrane surface and without damaging polymer with very small nanoparticles.	[18] [29]
Direct use of Evonik P25	PVDF, AA and TiO_2 (P25)	Direct attachment of photoactive P25, shows higher photoactivity of membrane.	Require surface functionalization to anchor TiO_2. Nanoparticles agglomerate and reduce the antifouling property of membrane.	[17]
	PVDF, PVA and TiO_2 (P25)			[19]
	PVDF, PDA and TiO_2 (P25)			[20]
	Electrospun nanofibrous PVDF nanomat, KOH, TiO_2			[14]

1.2.2 TiO_2 blended PVDF membranes (Mixed Matrix Membranes, MMMs)

The TiO_2 blended PVDF based MMMs can be prepared by adding P25 TiO_2 nanoparticles [22] [23] [25] [32] [33] or TiO_2 precursor, for example, tetrabutyl titanate (TBT) [34][35] together with PVDF solutions. Most of the studies fabricated TiO_2/PVDF mixed matrix membranes from TiO_2 nanoparticles contained polymer solutions by glass support solvent casting (Fig. 3) for preparing flat membranes [33] or extrusion to have hollow fiber membranes [32][23]. The final membrane structure can be achieved either by solvent evaporation (Fig. 3) or by the non-solvent induced phase separation method.

Membrane casting solutions are prepared by dissolving PVDF in a solvent, such as N, N dimethylacetamide (DMAc) [25], n-methylpyrolidone (NMP) [23][32][36], or triethyl phosphate (TEP) (a non-toxic solvent) [22], etc. In some studies, a second polymer, for example, PMMA [22], was added to the casting solutions to facilitate the phase inversion process and easily modify the membrane's structure and properties [22]. Besides, copolymers of PVDF, for example, Poly(vinylidene fluoride-trifluoroethylene), (P(VDF-TrFE)) [33], Poly (vinylidene fluoride-hexafluoropropylene) (PVDF-HFP) [37] , etc. are also used to improve membrane performance

such as self-cleaning properties. Porous membrane structure was fabricated by adding a pore-former, for example, polyvinyl pyrrolidone (PVP) [23] [32] to the membrane casting solution.

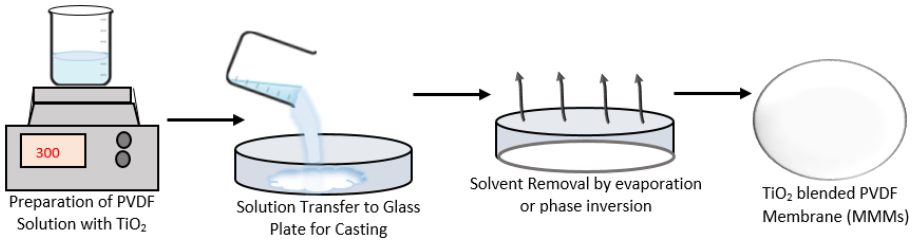

Fig. 3 Solvent casting in a glass support for TiO_2 embedded MMMs

For TiO_2 blended mixed matrix photocatalytic membranes, having a high exposed catalyst site on the membrane surface is still a challenge. Recently, electrospinning has attracted many studies because of the high surface area of the ultrathin polymeric fibers with diameters in the submicron to the nanometer range generated from this process. Therefore, it is possible to anchor a large number of photocatalysts within the electrospun nano-mat matrix [38]. During the electrospinning process, by applying a high voltage potential (10–40 kV) between the injector and the grounded collector, an electrically charged jet is created from a pendent of polymeric solutions generating ultrathin polymeric nano-fibers. After accumulations of ultrathin nanofibers on the collector an electrospun nano-mat matrix is formed (Fig. 4) [39].

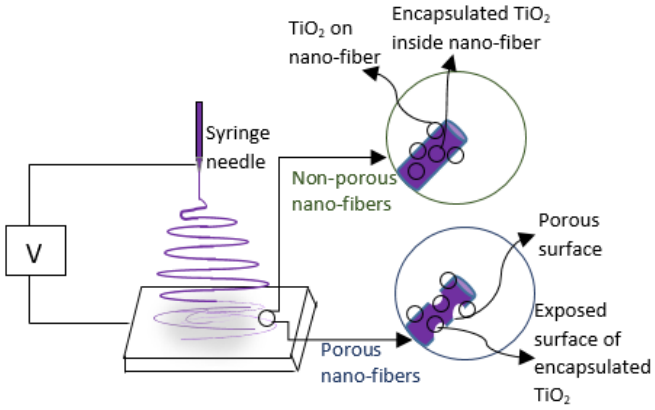

Fig. 4 Fabrication of TiO_2 anchored electrospun nano-fibers

To fabricate TiO_2 blended PVDF nano-mat, TiO_2 nanoparticles (P25)[36] [37], or TiO_2 precursor [34] can be added to the polymeric solutions. Compared to the TiO_2 nanoparticles blended electrospun membrane, the TiO_2 precursor based membrane provides more homogeneous TiO_2 nanoparticles distribution [34][36]. Nonetheless, further hydrothermal treatment is needed to crystallize the precursor based in-situ synthesized amorphous TiO_2 nanoparticles [34]. In both cases, either TiO_2 P25 or precursor blended electrospun PVDF membrane nano-mat still shows

some reduction in the active catalyst surface because some TiO_2 nanoparticles encapsulated inside the nano-fibers (Fig. 4) [34][37][38].

Fabrication of porous electrospun nano-fibers can overcome catalyst surface loss related issues of the electrospun membrane (Fig. 4). Past studies prepared porous nano-fibers by using the phase separation method to evaporate the volatile solvent, or by controlling electrospinning conditions, or by polarizing the prepared nano-fibers by heating and stretching in an electric field [40]. However, recent studies prepared a highly porous electrospun nano-mat by using a bi-polymer solution system (PVDF/PVP) and later removal of the sacrificial polymer (PVP) by further treatment, for example, polymer dissolution can yield more porous nano-fiber structures as well as more exposed catalytic sites [36]. A concise study and examples of PVDF blended TiO_2 based mixed matrix membranes (MMMs), activated under UV illumination, is shown in Table 2.

Table 2 UV activated photocatalytic membrane –TiO_2 blended PVDF mixed matrix membrane

Preparation Method	Polymer as a matrix, solvent or P25 TiO_2 or TiO_2 precursor	Advantages	Disadvantages	Ref.
Extrusion using one spinneret	PVDF, NMP, and TiO_2, PVP as a pore former [32], anionic surfactant SDS [23]	Greater mechanical stability, and reduction in membrane fouling.	Poor dispersibility, and entirely enfolded TiO_2 nanoparticles in polymer matrix decreases the photocatalytic efficiency.	[32] [23]
Co-extrusion using triple orifice spinneret	Inner layer: 18 wt% PVDF and 82 wt% of DMAc , and outer layer: 15 wt% PVDF, 3 wt% TiO_2 and 82 wt% DMAc			[41] [42]
Solvent Casting (non-solvent induced phase separation)	PVDF, DMAc, and TiO_2			[24] [25]
Solvent casting of the solution of copolymers (Phase inversion method or solvent evaporation)	PVDF/PMMA, TEP, TiO_2.	Addition of a second polymer facilitates the modification of membranes structure.		[22]
	P(VDF-TrFE), and N, N-dimethyl formamide (DMF), and TiO_2			[33] [21]
Solvent casting on glass plate (Phase inversion method)	PVDF, DMAc, LiCl, TiO_2	Reduced membrane fouling.		[43]
Solvent casting on plate of planographic coating machine	PVDF, PVP, DA, DMAc, TiO_2	Improved hydrophilicity and homogeneous distribution of catalyst.	A decrease in membrane flux due to reduction in pore size.	[44]
Solvent casting (solvent evaporation method)	PVDF-HFP, DMF, TiO_2, or Ag-TiO_2	Well distributed microstructures. No agglomeration of nanoparticles.	Time consuming solvent evaporation method.	[37]
Electrospinning		Smooth surface of nanofibers with homogeneous nanoparticles distribution.	Photocatalytic efficiency reduced due to encapsulation of catalysts inside the nanofibers.	
Electrospinning + hydrothermal treatment	PVDF, DMF, acetone, tetrabutyl titanate for TiO_2	A homogeneous distribution TiO_2 and visible-light responsive catalyst.	Require low temperature crystallization of TiO_2.	[34]
	PVDF, DMF, TBT, g-C_3N_4	Excellent self-cleaning properties, and good visible light driven PMs.		[35]
Electrospinning (NIPS) + Removal of PVP	PVDF/PVP, DMF, acetone, TiO_2	More exposed catalytic sites due to porous fibers (removal of one polymer).	An uneven distribution of TiO_2 and nanoparticles agglomerates.	[36]

1.3 Photocatalytic Membrane Reactors (PMRs)

To study the performance of the above-explained (section 1.2) UV responsive TiO_2 immobilized PVDF membranes, most of the researchers have applied them to photocatalytic

membrane reactors (PMRs) to treat the synthetic water. To date, TiO_2 based PVDF PMRs acted as a contactor reactor to degrade organic pollutants from synthetic wastewater. The effective removal of organic pollutants, as well as membrane photocatalytic efficiency, depends on the appropriate design, configuration, and operative conditions of PMRs [45].

1.3.1 Design and Configuration of PMRs

TiO_2 immobilized PVDF based PMR consists of a photocatalytic membrane reactor module and an illumination system. Most of the cases, researchers conducted batch operations to study the photocatalytic kinetics (Fig. 5a) [15][16][18][20][29][33]; however, some of the studies also performed continuous experiments mainly in modules with flat sheet membranes (Fig. 5b,c) [41][42][6].

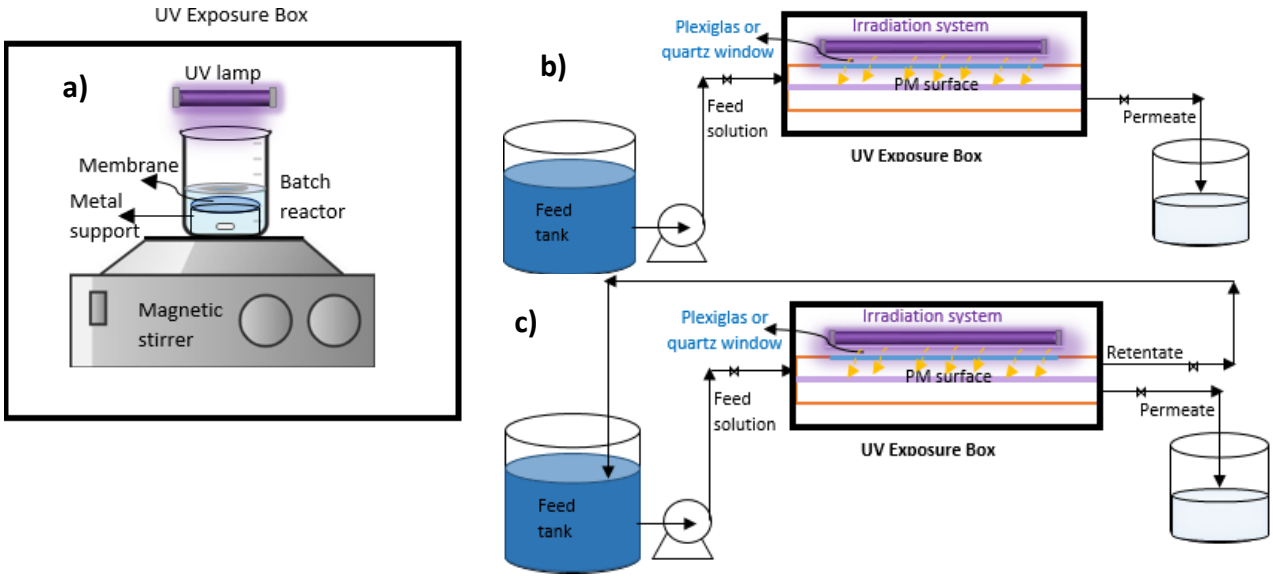

Fig. 5 Lab-scale operations of PMRs; a) Batch process; and (b,c) Continuous process; ((b) dead-end mode; (c) cross-flow mode)

In continuous operations of PMRs, the photocatalytic membranes can operate in dead-end mode (Fig. 5b) or cross-flow mode (Fig. 5c) [6]. In the case of dead-end mode, the feed solution passes through the PM surface, acting as a contactor, while the feed flow direction is parallel to the PM surface in case of cross-flow. Therefore, the probability of cake layer formation on to membrane surface is high in dead-end mode, resulting in a reduction in photocatalytic efficiency [46] with issues of membrane fouling [1]. In cross-flow mode, the tangential flow tends to remove the deposited particles on the membrane surface, and reducing the possibility of membrane fouling. The retentate is recirculated to the feed tank and permeate flows perpendicularly across the membrane (Fig. 5b). Besides, the recirculation system provides higher turbulence in the solutions, which in turn promotes the pollutant mass transfer from the bulk feed solutions to the catalytic sites

of the PM surface [1][46][47]. Thus, compared to the dead-end mode, the cross-flow mode would be feasible for most of the large-scale industrial applications [45][46].

During the consideration of the starting set-up of a PMR, for an efficient photocatalytic reaction, the whole PM surface must be accessible to irradiation. Besides, to promote the electrons from VB to the CB, the PM surface must be irradiated with the photon energy (h) equal to or higher than the bandgap [45]. Generally, in the lab-scale PMRs, light source (lamp) is on the top of the membrane unit with a quartz or Plexiglas window (Fig. 5b,c) or around the membrane module outside the reactor [47]. As TiO_2 photocatalyst is sensitive to UV light, researchers used different types of artificial UV source to irradiate the TiO_2 based PM surface. The mercury vapor fluorescent lamps with low pressure (LP) or medium pressure (MP) are the most used UV light sources. However, these lamps raise some problems during the applications, for instance, reduced footprint, higher maintenance, high energy consumption, and high heat generation increasing the solution temperature. [47]. Light emitting diodes can be an alternative source for PMR applications as LED can emit different wavelengths (near UV, infrared, or visible) based on the composition and condition of the lamp fabricating semiconductor (gallium arsenide, gallium phosphide etc.) materials. Besides, there are some advantages of using LED, for example, no disposal problem (no mercury), small in size, more durable (no glass or filaments), faster startup time, energy-efficient and longer lifetime, etc [47]. Moreover, xenon lamps, the closest in quality to the sunlight of all artificial light, are used as a solar simulator for PMR studies; however, some studies also used direct sunlight [47].

Recently, photocatalytic membrane micro-photoreactors [48], a new design of PMR, has been proposed in several studies. In this case, the reactor module consists of two concentric Plexiglas tubes with a tubular membrane inside and irradiation system (UV lamps) placed outside the reactor. In this case, the feed solution flows through the shell side and the permeate slips along the internal surface of the membrane and then exit through the tube side [6]

1.3.2 Effect of operating conditions

The operating conditions can influence the performance of TiO_2 based PMRs. The main operating parameters are light wavelength and intensity, pH, temperature, and feed flow, etc.

UV light, absorbed by TiO_2, generated from the sunlight, occupies only 4-5% light of total irradiations for an effective photosensitization process [49]. Therefore, the wavelength and photon

flux of applied light needed to consider, and it is salient to use an artificial light that can provide a higher photon flux [46].

Light intensity, a key factor during PMRs operation, can be categorized into three groups. 1) At low intensity (0-20 mW/cm^2), the reaction rate increases linearly with light intensity. Because, at this stage, the electron-hole generation is predominant, while electron-hole recombination is negligible. 2) At medium intensity (20-25 mW/cm^2), the electron-hole pair separation and recombination compete, and the reaction rate depends on the square root of the light intensity. 3) At high intensity (>25 mW/cm^2), the reaction rate becomes independent of intensity until it is not too high to limit the mass transfer. Because, the rate-limiting step of photocatalysis, the electron transfer from catalyst to oxygen leads to the generation of O_2^*, affected at higher intensity radiations [50][46][49][45].

The isoelectric point (PZC) of TiO_2 can vary from 6-7.5 [49]. Therefore, changing the pH of the polluted feed water, the condition of the ionization state of the TiO_2 surface and the position of VB, and CB of the TiO_2 can change. Consequently, the amount of generated hydroxyl radicles can be altered with pH and affect the photocatalytic reaction [44][51][49]. At alkaline conditions (pH>PZC), the positively charged pollutants can adsorb on the TiO_2 surface, while in the acidic states (pH<PZC), negatively charged contaminants are adsorbed [52][45]. Besides, the alkaline solution enhances the process efficiency [53] because this condition favors OH^- formation around the TiO_2 and hence generates more ROS [49]. Therefore, it is necessary to optimize the pH of the polluted water during the operation of the PMR.

Most of the PMRs studies conducted at room temperature suggested an optimum temperature range for TiO_2 based photocatalytic reaction between 20 and 80 ºC. Above this range (>80 ºC), the recombination of charge carriers is promoted, which is not suitable for photocatalytic reaction. Also, above 80 ºC exothermic adsorption of pollutants becomes unfavorable, while degraded product desorption becomes the limiting step below 20 ºC. Moreover, within this temperature range (20-80 ºC), the increase in temperature can enhance the photocatalytic activity by increasing the mass transfer rates (adsorption of pollutants and desorption of degraded products) and increasing the turbulence by decreasing the viscosity at higher temperatures [45][46][49].

Feed concentration, velocity, and presence of oxidants and ions in solution can affect the photo-degradation process of PMR. Increasing feed concentration within a limit can improve the photocatalytic reaction rate. A further increase in pollutant concentration can show a negative effect

on photo-degradation [53]. The higher concentration opaque solution can be an obstacle for the incident light to reach the photocatalyst surface of PM (light scattering by dissolved contaminant) or can saturate the active catalyst sites by occupying them. Aoudjit et al. [32] increased the tartrazine concentration from 10-30 mg/L in their study and observed a decrease in photo-degradation from 78% to 46%. For PMR, the presence of inorganic salts in feed solution can influence both the photocatalytic reaction and the membrane performance. The presence of inorganic ions such as Cl^-, CO_3^{2-}, NO_3^-, SO_4^{2-}, and HCO_3^- inhibit the photocatalytic activity by scavenging holes (h_{CB}) and hydroxyl radicals ($^*OH$) [44]. However, some other ions, for instance, $S_2O_8^{2-}$, BrO^{3-}, ClO^{2-}, ClO^{2-}, and IO^{4-} can act as a scavenger for the CB electrons, reducing the electron-hole recombination as well, and finally improves the photo-degradation [46]. Besides, inorganic ions can deposit on membrane surface resulting in reduction in permeate flux and serious fouling of membrane surface [45][46]. Dissolved oxygen, electron sink of photogenerated carriers [45], can intensify the photocatalytic reaction [49]. Controlled aeration rate can be an alternative; because turbulence or air bubbles generated from higher aeration rates can hinder the photodegradation [45]. PMR requires proper mixing to transfer the pollutants from the bulk of the liquid to the photocatalyst surface [47]. Some studies applied the cross-flow mode (recirculation) in PMR to improve the photodegradation efficiency [1].

1.3.3 Reaction kinetics

In most of the PMR studies, the Langmuir-Hinshelwood mechanism [54][50][22][45] the kinetic equation to describe the degradation rate as a function pollutant concentration, and the total rate of reaction follows the equation below.

$$-\frac{dC}{dt} = -r_A = \frac{k_r K_{ads} C}{1 + K_{ads} C} = \frac{k_{app} C}{1 + KC} \quad \text{.....} \quad 1$$

where, r_A is the rate of degradation of the pollutant (mg/min); C the pollutant concentration (mg/L) at time t; k_r is the intrinsic rate constant (mg/(L×min)) and K_{ads} is the adsorption equilibrium constant (L/mg) or binding constant. When the adsorption is relatively weak or for lower concentrated solutions, eq. 1 can be simplified as a pseudo first order kinetics with an apparent constant of degradation, k_{app} (min^{-1}) as shown below, where C_0 is the initial pollutant concentration.

$$ln\left(\frac{C}{C_0}\right) = k_r K_{ads} t = k_{app} t \quad \text{.....} \quad 2$$

1.4 Photocatalytic Activity and Membrane Performances

Most of the TiO_2/PVDF based PMs are UV-sensitive, and hence used to decompose organic pollutants in wastewater. These PMs combine the photocatalytic degradation and filtration of contaminated water/wastewater under UV-light. Besides this, incorporation of TiO_2 with PVDF present several attributes to other membrane performances, such as hydrophilicity, antifouling, and self-cleaning property, the permeability of the membrane, etc. over conventional membrane separation. In general, conventional systems suffered from membrane fouling due to the deposition of the fouling agents on membrane surface and hence decreased permeation of flux and membrane life as well as the increase in energy consumption and treatment cost. Nevertheless, in the case of PMs, pollutants in the feed solution are degraded by the generated ROS from photocatalysts under illumination exactly on the membrane surface. Therefore, less probability of forming cake layer on the membrane surface, reducing pore blocking, hindering membrane fouling to some extent and improve permeate quality. Also, reducing pump consumption to extract permeate and membrane cleaning frequency.

TiO_2 based PVDF membranes are mainly tested for dye removal, BSA filtration, removal of phenolic compounds (bisphenol A) or other natural organic matter rejections, etc. These membranes are also studied for photobacterial effect under UV-irradiation. In this case, Escherichia coli is generally selected as an indicator. It was reported that under UV-light, bacterial cells show an irreversible damage to not-culturable state on the PMs [49]. However, the photocatalytic activity and other performances of the PMs depend on the TiO_2/PVDF PMs fabrication method, and added amount TiO_2 etc. Incorporation of TiO_2 with PVDF can enhance the thermal, mechanical and self-cleaning properties with the photocatalytic activity of the membrane. Increasing TiO_2 loading within the PVDF membrane increase the hydrophilicity and antifouling property of membrane. However, the amount of added TiO_2 within the membrane is needed to optimize for the overall performance of the membrane. Because above this optimum content, instead of improving, some of the membrane performances even significantly reduced. The reason is that abundance of TiO_2 nanoparticles can agglomerate and block the membrane pores [28] and hence reduced porosity, which is closely related to membrane water flux [44]. For example, PVDF membrane coated with 1.5 wt% TiO_2 exhibit more hydrophilicity, but 0.5% TiO_2 coated PVDF had a higher flux of 1% aqueous BSA filtration [28]. Annex 2 shows an outline of the representatives of some UV-

responsive TiO_2/PVDF based PMs, the optimum TiO2 content for better photodegradation activity and performances of the membrane.

Developing visible-light-driven TiO_2 based PMs may be an effective approach to avoid high energy consumed UV-lamp. Some emerging modification methods, for example, doping of metal (e.g., Ag, Fe, Cr, Co, Mn, V or Mo) or nonmetal (eg. N, B, carbon materials) [11][55], co-doping, coupling with another semiconductor (TiO_2/ZnO), and developing composites with carbon materials are recently used to prepare visible-light sensitive TiO_2 with reduced band-gap and slower recombination rate of photo-generated charges [55][56]. This modified TiO_2 can be incorporated with membranes to fabricate visible-light sensitive PMs [11]. Anchoring of such modified TiO_2 not only shift PMs photo-sensitivity to the visible-light region but improve other membrane properties. However, in some cases, modified TiO_2-based membranes shows better antifouling properties and antibacterial properties than TiO_2-based membranes [57][58]. Incorporation of Ag-doped TiO_2 within PMs, increase antibacterial activity of membrane with shifting the sensitivity of membrane towards visible light. Small TiO_2 nanoparticles show intracellular damage, while Ag has the unique antibacterial property and Ag-doped TiO_2 based PMs has excellent antibacterial and self-cleaning properties under visible-light irradiation [52] [59]. Inclusion of RGO with Ag-doped TiO_2 based membranes, the rejection performance and water permeability of membrane enhanced [58]. In the case of visible-light responsive PMs, likewise, TiO_2 loaded membrane, the amount of modified TiO_2 content within PMs is also an important factor for PMs photocatalytic activity and other performances. Higher content of modified-TiO_2 increase the mechanical properties [60], but at the same time membrane roughness increased and porosity decreased due to nanoparticle agglomeration [61][55][62], resulting in decreased membrane flux and antifouling ability [62]. Thus, photosensitivity and other performances of modified TiO_2-based visible-light responsive PMs depend on type and property of modified-TiO_2, the fabrication method of used for PMs, and the amount of modified TiO_2 added.

Studies on the fabrication of visible-light responsive PMs are still relatively limited, and only a few of them are based on polymeric membranes. Annex 5 summarized some of the TiO_2/polymeric based visible-light-driven PMs incorporating modified-TiO_2, the effect of the amount of added modified-TiO_2 on the performances of PMs, and an optimum dose for each PMs.

1.5 Challenges and Future Perspectives of Photocatalytic Membrane Reactors

The main challenges of PMRs are primarily related to the development of visible light-activated photocatalytic membranes and optimal reactor configurations to improve PMRs efficiency. Also, an important issue, as in any other application from lab to real operation, is to study the effect of real-time wastewater on membrane performance.

Many studies extensively used TiO_2 immobilized UV-responsive photocatalytic membranes lab-scale experiment for wastewater treatment, disinfectant, and pollutant removal, while studies on visible light-responsive PMs to date are still limited. Using UV lamps to sensitize TiO_2 for photocatalytic performance is expensive as they consume high amount of energy; hence, PMRs are still facing competition from conventional systems as they may be cheaper in terms of operational costs [47]. The high photo-efficiency of the TiO_2 under UV light limits the use of solar energy as the UV range is less than 7% of the solar spectrum [63][11], and hence the maximum percentage of light left as unused. The fast recombination of photogenerated charges from TiO_2 results in poor photoactivity under visible light [11]. Also, during the operation of PMRs, because of the reduced illuminated catalyst surface area per volumetric water treated, and higher rates of photon scattering, the efficiency of PMRs can be reduced [3]. Besides, using less expensive polymeric membranes faced difficulties because polymeric membrane structure can show fragility by both UV light and reactive oxygen species (e.g., •OH) [11] [45]. The more preferred polymers for the photocatalysis applications can be highly fluorinated, for example, PTEF and PVDF, which show more resistance to UV irradiation and oxidative (H_2O_2) environment [11]. These fluorinated polymers can also be sensitive to long-term UV exposure, while visible light will not cause damage to polymeric membranes [64]. Visible-light activated PMs will provide the guarantee of stability [11] and will be a probable solution from the energy point of view [45] [49]. Various researches are going on to fabricate visible light-sensitive PMs by incorporating modified TiO_2 (see section 1.4 and Annex 5), which can use the greener light source (the sun) or less energy consumed LED technology for large-scale applications.

Most of the researches on PMRs are mainly focused on materials development and overlook the improvement of photocatalytic performance by innovative reactor design and configurations and thus researches on reactor design, kinetics, modeling, and simulation remain in the conceptual phase [3][47]. Two concepts are needed to consider during an innovative reactor configuration; uniform distribution of light and effective mass transfer of pollutants to the photocatalytic surface.

In the latter case, researchers devoted to fabricating PMs with appropriate porosity and effective dispersion of photocatalysts. For a uniform light distribution with the highest quantum efficiency, lighting setup should be in such a way that every piece of PM's surface can be irradiated. A bundle or series of LED lights can be considered for an efficient illumination system [47]. Recently, micro-photoreactors concept used in PMRs research for a better illumination system [48]. Also, solar-powered PMRs shows prospect for purposes of pretreatment or after treatment of other advanced oxidation processes, treating small-volume waste streams from aquaculture and hydroponics or detoxifying of treated drinking water [3]. Recent research is underway to couple PMRs with other membrane techniques, for instance, coupling photocatalysis with membrane distillation, photocatalysis with dialysis, and photocatalysis with pervaporation [45].

Finally, PMRs based lab-scale studies used synthetic water, for example, dye solution or other organic solution as a contaminated source, hence still facing challenges for the large scale set up and practical applications. To translate the lab-based PMRs studies into practical applications, the use of real-time wastewater is mandatory, because, real wastewater contains inorganic salts, suspended solid particles with organic dissolved pollutants. Besides, in real cases, pollutant type, pH, temperature, etc. can be varied and have effects on PMRs performance. Therefore, scaling up the PMRs technology and optimize the reactor configuration for better performance at an industrial level, more research on PMRs should be done to study pilot-scale PMRs using real wastewater [1].

2. Objectives of this work

The main objectives of this work are:

- To prepare TiO_2 coated PVDF PMs using a facile sol-gel synthesis method, and transform the in-situ synthesized TiO_2 to photoactive anatase phase via low-temperature hydrothermal treatment.
- To fabricate a highly porous TiO_2 blended PVDF incorporating TiO_2 P25 with a bipolymer system using electrospinning process.
- To characterize and evaluate the photocatalytic performance of both TiO_2 coated and TiO_2 blended photocatalytic membrane.

3. Experimental

3.1 TiO_2 coated PVDF membranes

3.1.1 Membrane synthesis

We selected 47 mm diameter hydrophilic polyvinylidene fluoride (PVDF) membranes (Merck Millipore Ltd.) with 0.1 µm pore size to deposit TiO_2 nanoparticles on the membrane by sol-gel synthesis process. For this purpose, we prepared a series of 20 mL sol-gel solutions containing different concentration (2, 4, 8, 16, and 32 mmol/L) of titanium (IV) butoxide (TIB) (99%, Sigma-Aldrich) by adding 13.5, 27.2, 55, 110 and 220 µL of TIB in 20ml absolute ethanol (EtOH) (99.8%, AppliChem Panreac). We named the sample membranes as per concentrations used for coating and the number of membranes prepared in the same conditions. For example, without coated one 0mM, membrane 1 coated using 8 mmol/L TIB solution is 8mM1, and so on.

Before starting the reaction with the sol-gel solution, we pretreated the weighted PVDF membrane by immersing 30s in EtOH, 1 min in 50% EtOH, and 2 min in ultrapure water (Milli-Q) (Fig. 6) and then hold the membrane vertically for 10s to drip off the water. We placed the membranes in individual Petri dishes containing the TIB solution for 5 min to occur the reaction onto the PVDF membrane. After that, we rinsed the membranes with ultrapure water for at least 30 min three times and finally air-dried [16].

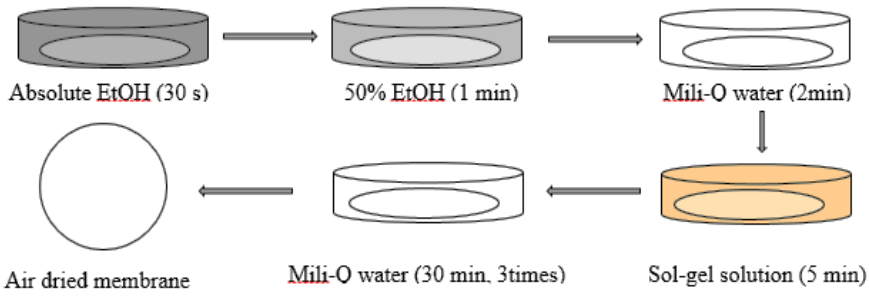

Fig. 6 Schematic representation of in-situ sol-gel synthesis method to deposit TiO_2 on PVDF membrane

3.1.2 Crystallization of TiO_2

The as-prepared sol-gel synthesized TiO_2 nanoparticles on the membrane were in the amorphous state [31], therefore, low-temperature hydrothermal treatment (LTHT) was needed to crystalize the TiO_2 [16]. To establish the conditions for the LTHT, we prepared powdered TiO_2 nanoparticles from titanium tetra-isopropoxide (TTIP) (97%, Sigma-Aldrich). We mixed 6 mL TTIP and 10 mL absolute EtOH in a beaker, stirred and dropwise added 1 ml ultrapure water. After that we washed and separated the prepared nanoparticles with water by 1 min sonication and 10 min centrifugation at 10000 rpm; we did the same procedure twice. We dried the wet TiO_2 nanoparticles in an oven at 70 ˚C overnight. To study the LTHT, we took 2 mL of water at the bottom of a closed recipient (Nalgene, Polypropylene) (Annex 6) and 50 mg of as-prepared TiO_2

powder in a watch glass. Then we placed watch glass inside the recipient in such a way that water was not in direct contact with TiO_2 powder; two sealed recipients were heated at 110 ˚C for 3.5 hours and 72 hours respectively. To crystallize the TiO_2 deposited on membranes, we performed the same LTHT experiment (Annex 6) for 3 hours at 110 ˚C and to ensure that enough amount of water was present, which represents more than four times of the ratio of water/TiO_2 added in case of the powder [16].

3.2 Electrospun phototcatalytic membranes

3.2.1 Fabrication of Electrospun PVDF Nano-fiber Membrane

We collected pure PVDF electrospun membrane from a previous project and it was prepared by Shadi Alnahari (EM3E-4SW student, 3rd Edition) within the frame of his individual project at the University of Zaragoza, according to the following recipe based on previous results in the lab [65]. the preparation procedure is as follows: 10 wt% PVDF solution was prepared by dissolving 1110 mg PVDF powder (Solef® 6012, Solvay) in 12 ml mixture of Dimethylformamide (DMF) (99% Fisher Chemical) and Acetone((99%, Acros organics) (mass ratio of DMF : Acetone = 6:4). Then, added 5 mg of Lithium chloride anhydrous (LiCl) (Fisher Chemical) to the solution and stirred at 70°C overnight. That solution was used to fabricate PVDF nano-fiber membrane with an electro-spinner (Yflow Electrospinner 2.2.D-500, Spain) consisting of a syringe pump, a control panel, and a power supply (Fig. 7b).

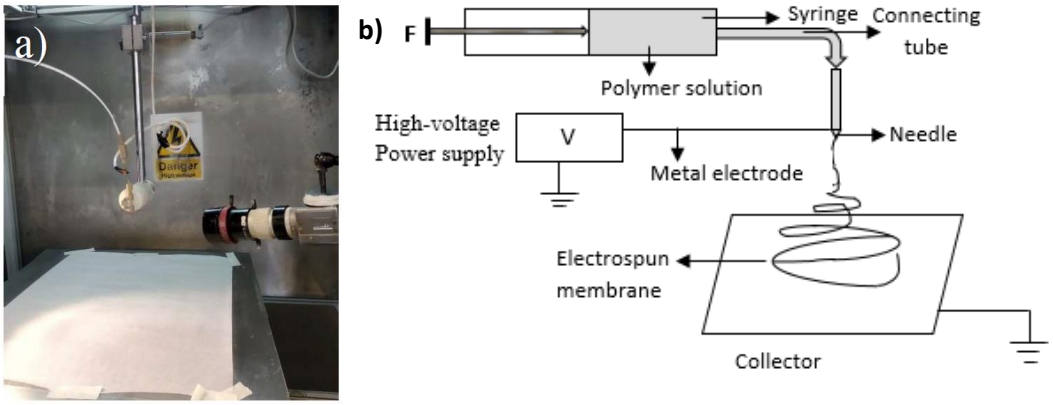

Fig. 7 Experimental (a) and Schematic (b) setup of Electrospinning process.

The polymeric solution was taken in a 15.9 mm internal diameter syringe and pumped it through a connecting tube to reach the tip of a needle with a flow rate of 1 ml/hr (Fig. 7b). A high voltage was applied between the tip of the needle and the collector to form nanofibers. The collector voltage was adjusted as –2 kV with +16 kV for the emitter and a 15 cm distance was maintained between

the needle and the parchment paper, placed on the counter electrode (Fig. 7a). To control the motion, the stroke for left-right motion was fixed 80 mm while 150 mm for back-front motion. The electrospinner was running for 8 hours and the fabricated membrane was collected. The newly prepared electrospun PVDF membrane was dried at 100 °C for an hour and kept it between two flat plates in an oven at 130 °C overnight.

3.2.2 Fabrication of Electrospun PVDF/TiO_2 Nano-fiber Membrane

To fabricate a PVDF/PVP/TiO_2 Electrospun Nano Fiber Membrane, we dissolved 1330 mg (12 wt %) PVDF and 665 mg (6 wt %) Polyvinylpyrrolidone (PVP) (Sigma-Aldrich, average MW= 40 000) in a 10 ml (8.62 g) equal volume mixture of N,N-Dimethylacetamide (DMAc) (99% Sigma-Aldrich) and acetone with 440 mg (4 wt%) TiO_2 (99.5%, Evonik P25). We stirred the solution at 60°C for an hour and continued it overnight at room temperature. We fixed the electrospinner settings as same as mentioned for the PVDF membrane except for the emitter voltage (+10 kV) (Fig. 7). After 8 hours of electrospinning, we collected the PVDF/PVP/TiO_2 nanofibers and dried in an oven at 90°C overnight to remove the residual solvent.

We washed the PVDF/PVP/TiO_2 membranes (PPTM) with water to dissolve the PVP polymer. The main goal of this is to expose more TiO_2 nanoparticles embedded inside the fibers. For this purpose, we immersed the PPTM nano-mat in deionized (DI) water and sonicated for one hour. Then we left the membrane in a water bath at 60 °C for 24 hr. To avoid the shrinkage of the membrane during drying, we placed the membrane between two flat plates and kept in an oven at 90°C overnight. To ensure complete removal of PVP, we repeated the washing process and obtained a PVDF/TiO_2 membrane (PTM).

3.3 Characterization of membranes

3.3.1 The Surface Morphology of Membranes

We characterized the membrane surface morphology by using a field emission scanning electron microscope (FESEM CSEM FEG INSPECT - 50). We prepared SEM samples by depositing a 14 nm palladium layer on TiO_2 coated PVDF membrane samples and a 20 nm carbon layer on electrospun membrane samples by the sputtering method.

3.3.2 TiO_2 nanoparticles loading in membrane

We estimated TiO_2 loading for TiO_2 coated PVDF membranes by measuring the membrane weight before and after the sol-gel synthesis. To evaluate the thermal stability, and to quantify the

TiO_2 loading in the electrospun membranes, we performed thermogravimetric analysis on a TGA instrument (TGA/SDTA851, JULABO heating circulator) with heating rate of 10 ºC/min under nitrogen flow from 35 ºC to 800 ºC. Taking TGA samples from the two different parts (side and middle) of the electrospun nano-mat, we distinguish the TiO_2 distribution within the membranes.

3.3.3 Nanoparticle Crystallization by hydrothermal treatment

To distinguish the crystalline conditions of TiO_2 powder and TiO_2 in membranes, we measured the X-Ray diffraction patterns of as-prepared powdered TiO_2 and hydrothermally treated TiO_2 (3.5 h and 72 h), and TiO_2 coated PVDF membrane (32mM) on an X-ray diffraction equipment (PANalytical EMPYREAN). Using the XRD pattern of powdered samples and applying the Debye Scherrer equation, we calculated the mean size (D) of the crystalline domains of samples. [Scherrer formula: $D = K\lambda/(w \times Cos\theta)$, where w is the width at half-maximum intensity, K is the shape factor (0.9), and λ is X-ray wavelength (0.15406 nm)].

3.3.4 Experimental set-up for Methylene Blue adsorption and photocatalytic degradation

To evaluate the photocatalytic performance of the TiO_2 coated PVDF membrane and Electrospun PVDF/TiO_2 membrane (PTM), we degraded Methylene Blue (MB) (≥95%, Fluka) as a model organic pollutant in batch processes under UV light. We used circular membranes for adsorption and degradation experiments; and hence cut the electrospun PTM nano-mat (PTM1, and PTM2 from the mid-portion, while PTM3 from the side) into a 47mm diameter circle as the same as the commercial membrane (see section 3.1). We performed the experiments under stirring to have good contact with the membrane and solution. To maintain the mechanical stability of the membrane under stirring, we attached them to a steel frame, containing a hollow circular opening, (Fig. 8a) with tape, and then placed in 70ml of 6.4 ppm MB solution. To find out the optimum stirring conditions for photodegradation experiments, we conducted MB adsorption experiments using non-coated PVDF membranes (0mM) by changing rotation speed from 200rpm to 400 rpm. For each trial, we set up the stirring conditions and then placed the membrane into MB solutions. We connected a rotary pump to continuously circulate the solution from beaker to cuvette of a UV-vis spectrometer (Agilent 8453) through connecting tubes to constantly (each 30s) record the concentration changed in the solution (Fig. 8b).

Before starting the photodegradation experiments, we prepared the MB calibration curve by measuring the absorbance values of seven different concentration (1-7 ppm) solutions. Using a

UV-vis spectrometer (Agilent 8453), we measured the absorbance values of MB solutions at 665 nm, corresponding to the maximum absorption peak for MB.

During the photodegradation experiments, at first, we kept the membranes-solution system under dark conditions for 120 min. Then, after reaching the adsorption-desorption equilibrium, we turned on the solar simulator (Zolix SS150) to initiate the photocatalytic reaction. We continuously monitored the solution concentration of the reaction system using a UV-vis spectrometer. The distance from the lamp to the membrane was 10 cm (for one sun), and the light intensity was 1000 W/m^2. We maintained the same experimental conditions for both TiO_2 coated PVDF membrane and TiO_2 blended electrospun PVDF membranes. To verify the reusability TiO_2 blended electrospun PVDF membranes, we repeated the photodegradation experiment twice more.

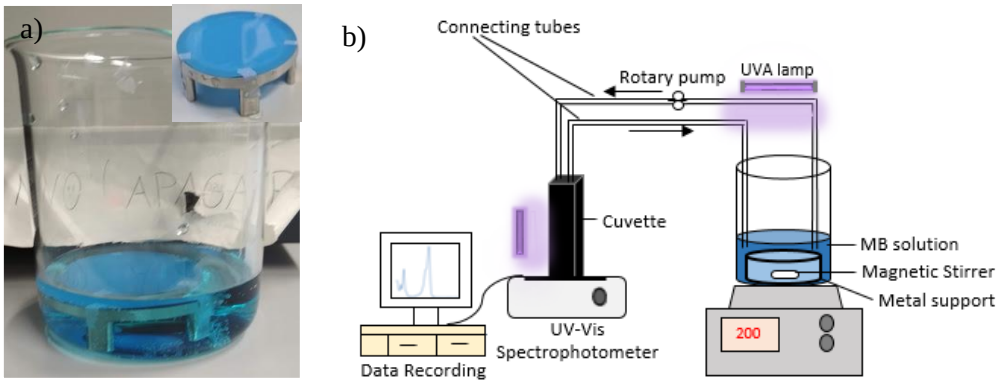

Fig. 8 (a) Experimental and (b) Schematic representation of MB photodegradation experiment.

4. Results and Discussion

4.1 TiO_2 coated PVDF membranes

4.1.1 Characterization and Surface Morphology

The pre-wetted (water-soaked for 2min) hydrophilic PVDF membrane was immersed directly in TIB/ethanol solution, and the surface water immediately started hydrolysis reaction to deposit TiO_2 on the membrane surface. The amount of TiO_2 deposited on membrane surface is shown in Table 3, and as expected, it increases with sol-gel concentration.

Table 3 Samples prepared by sol-gel with different concentrations of TIB as precursors and amount of TiO_2 nanoparticles deposited and % loading on membranes

Membrane	Nº of samples	Average Weight Gain (µg)	wt% TiO_2 loading	% TiO_2 synthesis yield
2mM	1	11	0.009	0.34
4mM	1	172	0.147	2.70
8mM	3	588±41	0.497	4.61
16mM	8	623±59	0.527	2.44
32mM	2	1166	0.984	2.28

The amounts of TiO_2 deposited for lowest concentrations, 2mM and 4mM, are 11 µg (0.009 wt%) and 172 µg (0.147 wt%) respectively (Table 3). In contrast to 2mM membrane, prepared by Fischer et al. [16] using the same method (sol-gel) and hydrophilic membrane, they obtained about ten times higher TiO_2 loading (0.092 wt% measured by TGA) on the membrane surface. Fischer et al. used TTIP as a precursor to prepare a 2mM sol-gel solution, instead of TIB in our case [16]. The probable explaining the lower loading could be the nature of the alkoxy group that influenced the induction period, which is increasing with the length of the chain; thus, the reactivity of TTIP is higher than TIB [31]. Besides, the calculated yield of TiO_2 of 2mM and 4mM membranes was 0.34% and 2.70% respectively; however, no visible TiO_2 nanoparticles were detected during SEM inspection of these membranes and surface morphology observed was the same as non-coated PVDF membrane (0mM) (Annex 7).

The quantity of TiO_2 deposited on 8mM and 16mM membranes (medium concentration sol-gel solution) were 588± 42 µg (0.497 wt%) and 623± 58 µg (0.497 wt%) respectively, and the estimated yield of corresponding membranes was 4.61% and 2.44% (Table 3). We observed an agglomeration-free and homogeneous deposition of TiO_2 nanoparticles in this case (Fig. 9). The average diameter of TiO_2 nanoparticles loaded on 8mM was 48.96 ± 31.07 nm (N = 141) (Annex 8a). The size of TiO_2 nanoparticles, anchored on 16mM, was increased, and had the average diameter of 67.47 ± 41.16 nm (N = 183) (Annex 8b).

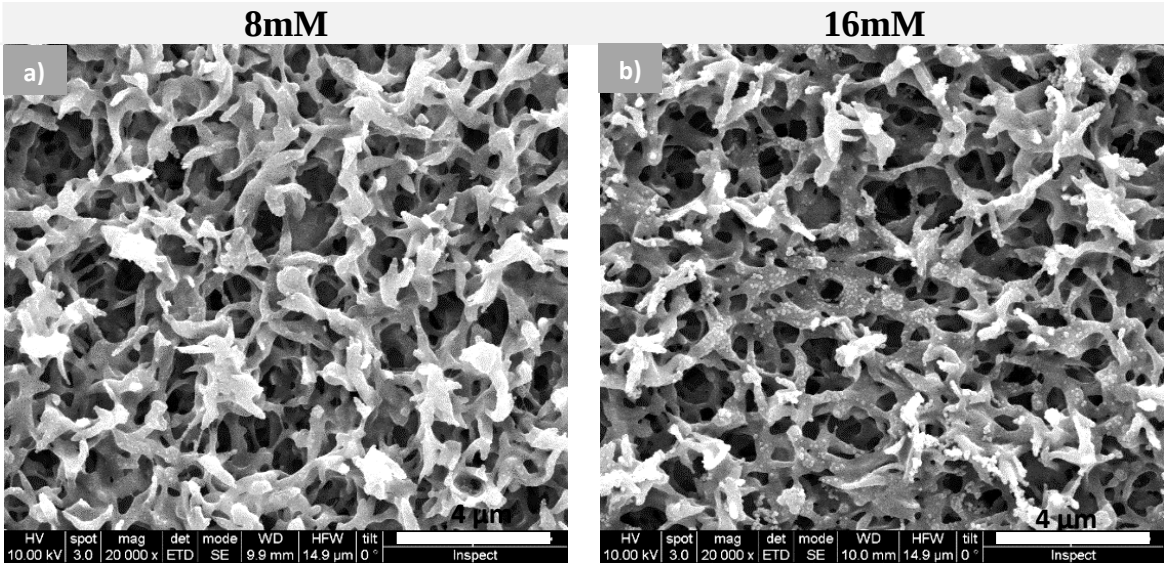

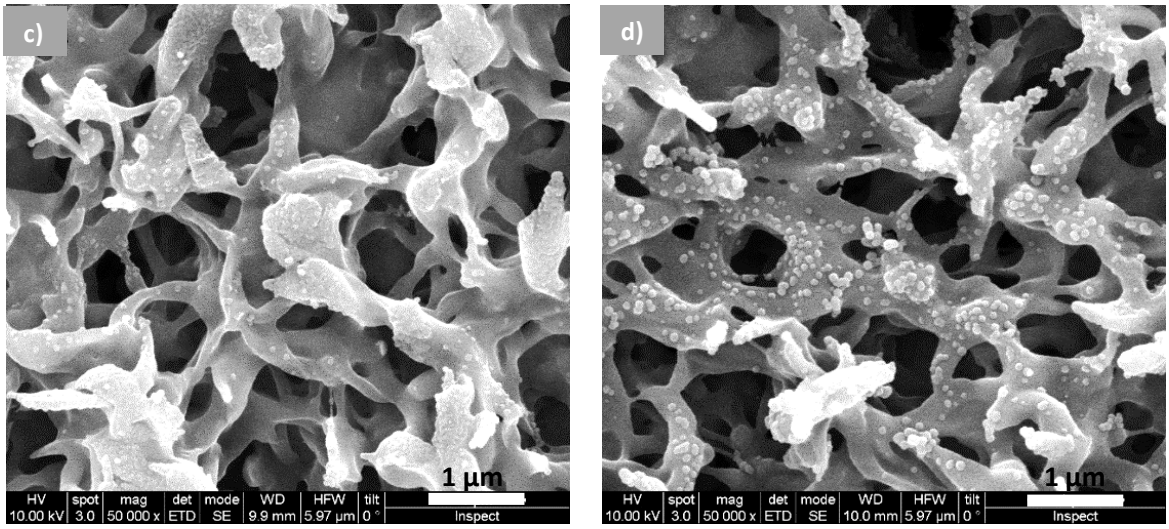

Fig. 9 SEM images of TiO_2 coated PVDF membranes prepared via (a,c) 8mM and (b,d) 16mM TIB sol-gel solution at different magnifications;

In the case of 32mM, membrane prepared from the highest concentration sol-gel solution, the estimated yield of TiO_2 was only 2.27%. Also, the amount of TiO_2 loaded on this membrane was 1166 µg, which is 0.984 wt% of the corresponding membrane (Table 3). In this case, there is a non-homogeneous distribution of TiO_2 nanoparticles along the membrane surface (Fig. 10a,b). The average diameter of TiO_2 nanoparticles anchored on 32mM was 108.15 ± 75.28 nm (N = 157), which is almost two times larger than TiO_2 nanoparticles on 8mM and 16mM (Annex 8c).

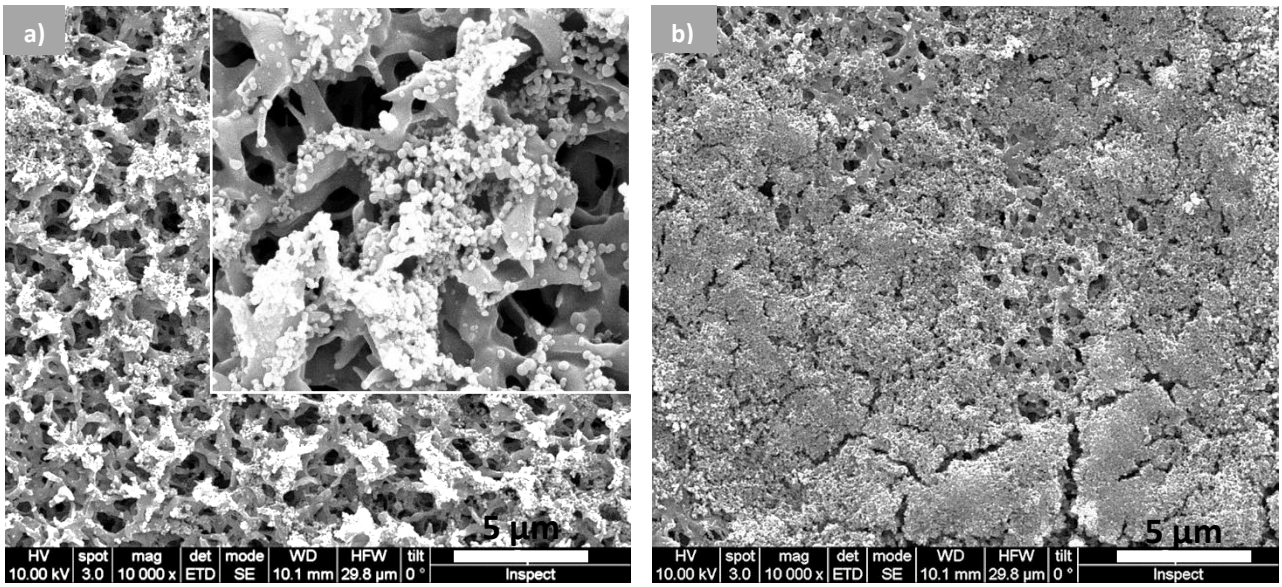

Fig. 10 SEM images of 32mM at different position of the sample (a,b) and its corresponding enlarged view of (a).

Applying a sol-gel dip-coating method, Hou et al. [15] obtained a layer of smaller and agglomeration-free nanoparticles on a hydrophilic PVDF membrane surface. They formulated a 1 M TTIP sol-gel solution with 0.5 M acetylacetone, as a chelator, and maintained pH at 1.2 by

adding Perchloric Acid ($HClO_4$), while in our case solution pH was 6-7. Compared to our results for 32 mM, Hou et al. [15] gained two times higher TiO_2 loading (1.9 ± 0.1 wt%) after the first cycle. The reason is that the size of the nanoparticles depends on the sol-gel solution concentration, pH, and the type of precursors used [31]. The average diameter of the TiO_2 synthesized from acidic sol-gel (pH≤ 3) is independent of precursors (TIB or TTIP), and 100 times smaller than the TiO_2 nanoparticles obtained from same concentrated neutral (pH=7) sol-gel [31]. Additionally, in the case of neutral sol-gel (pH=7), the size of the nanoparticles depends on the precursors. At these conditions, TiO_2 nanoparticles synthesized from TIB-based sol-gel are about 1.5 times larger than the nanoparticles from TTIP [31]. Therefore, the probable reason for agglomeration and non-uniform distribution of TiO_2 nanoparticle deposited on 32mM membranes could be the use of TIB precursor based neutral pH sol-gel. To prepare a TiO_2 coated PVDF membrane with an agglomeration-free uniform layer of TiO_2 nanoparticles, an acid catalyst and a stabilizing agent can be added to higher concentrated sol-gel solution. The anionic group of a stabilizing agent forms coordination bonds with Ti-ions in a bidentate chelating mode resulting in 6-membered rings stabilized by partial charge delocalization [66].

4.1.2 Crystallization results for hydrothermal treatment

The TiO_2 nanoparticles, synthesized at 25 ºC from sol-gel solutions, are not crystalline. Heating above 300 ºC can transform the prepared TiO_2 samples into a photoactive anatase crystalline structure [31]. However, in our case, nanoparticles are deposited on temperature sensitive-polymer support (PVDF, melting point 177 ºC). For this reason, we crystallized the deposited TiO_2 on membrane by low temperature hydrothermal treatment (LTHT) method, where in presence of water vapor, amorphous TiO_2 nanoparticles transformed into semi-crystalline anatase [67]. To establish the conditions of the hydrothermal treatment, we synthesized TiO_2 powder by sol-gel method using TTIP as precursor in this case and achieved a 95.5% synthesis yield. Nevertheless, different precursor (TIB, TTIP) based sol-gel solutions at the same conditions yield similar crystalline TiO_2 nanoparticles, and the observed differences are the nanoparticle size and surface area [31]. We studied the crystallinity of TiO_2 powder and TiO_2 coated membrane by X-ray diffraction analysis and the resulted patterns are shown in Fig. 11.

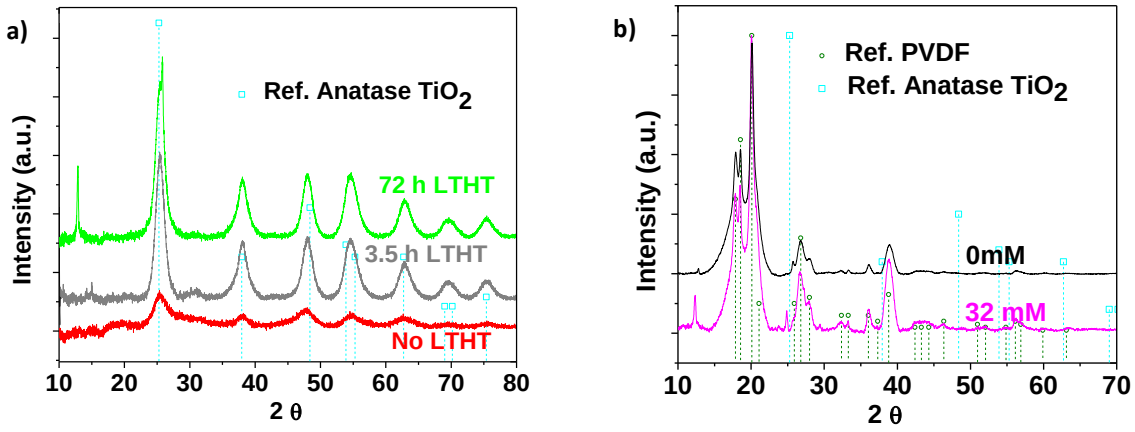

Fig. 11 XRD patterns of (a) as-prepared powdered TiO_2 (before and after LTHT) and reference anatase peaks; (b) 32mM membrane after LTHT, non-coated PVDF (0mM) and reference peaks of PVDF. (Lines stand for X-ray diffractograms and vertical lines with scattered points denote references)

The room temperature sol-gel synthesized wet TiO_2 particles at 25 ºC, were dried at 70 ºC for 12 h and then we performed LTHT to crystallize the dried TiO_2 powders. From the X-ray diffractogram (Fig. 11a) of TiO_2 powder before LTHT, we observed low intense broad peaks [67]. The evolving reflections, in the XRD of TiO_2 powder (Fig. 11a) before and after LTHT (3.5 hour and 72 hour), correspond to the diffraction peaks of anatase TiO_2 ((JCPDS no.21-1272, a=3.7852 Å, c=4.683 Å, space group: I41/amd (141)), and validates crystallization process via LHTH. We obtained almost similar sharper peaks for 3.5 h and 72 h hydrothermally treated TiO_2 powder. For 72 h LTHT TiO_2, there was a small peak reflected at $2\theta \sim 12$ º, which has not been identified.

The calculated mean size of the crystalline domains, using Debye Scherrer equation, are 3.6 nm, 5.2 nm, 5.8 nm respectively for dried TiO_2 powder, 3.5 h and 72 h hydrothermally treated powder respectively. Therefore, LTHT for 3.5 h and 72 h yields almost same size crystalline domain. To transform the in-situ synthesized TiO_2 on PVDF membrane to photoactive anatase phase, we carried out same LTHT for 2 h for our prepared membranes. From Fig. 11b, all of the intense peaks of the XRD patterns of both TiO_2 coated PVDF (32mM), and non-coated PVDF (0mM), are analogous to the peaks of α-PVDF (JCPDS no. PDF 00-042-1650, a=4.976 Å, b=9.59 Å, c=4.626 Å, space group: P21/c (14)), except one small intense peak at $2\theta \sim 25$º. This reflection matches with the TiO_2, and confirms the presence of some anatase TiO_2 on the membrane surface.

4.1.3 Adsorption and Photodegradation of Methylene Blue

Initially, we investigated the adsorption of methylene blue in non-coated PVDF membranes and studied the effect of agitation by changing the rotation of speed from 200 to 400rpm. The

standard deviation of the measured adsorption rate in three runs at 200 rpm was almost ±2% (see Fig. 12a). We found a similar error (±2.3%) when comparing the adsorption rate from different agitation speeds (Fig. 12b), and then we concluded that there are no effects of agitation in the range studied; thus, we selected rotation speed 200 rpm in the following photocatalytic experiments.

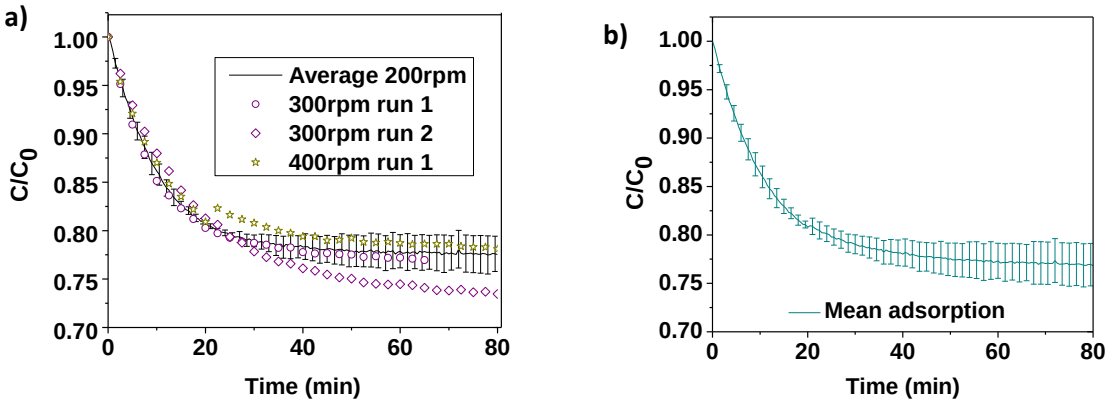

Fig. 12 Influence of agitation on adsorption of MB onto 0mM (a) Rate of adsorption of MB at 200 rpm for 3 runs (mean with error bars) , with 300 rpm (two runs), and 400 rpm(b) Average adsorption rate of MB at 200 rpm, 300 rpm, and 400 rpm with error bars.

We studied the adsorption of MB onto the TiO_2 coated membranes and compared them to the results of the non-coated 0mM (Fig. 13). We fitted the adsorption kinetics data to the following batch kinetics equation below and fitted values are shown in Fig. 13.

$$-\frac{dC}{dt} = -r_A = k_L \times a \times (C - C^*) = P \times (C - C^*) \quad \ldots\ldots\ldots\ldots \quad 3$$

where, C is the concentration of solute in the bulk liquid; C^* is the concentration in equilibrium with the adsorbent loading; k_L is the external liquid-phase mass-transfer coefficient; a is the external surface area of the adsorbent per unit volume of liquid; and P is termed as global adsorption kinetic constant which is the product of k_L and a. Performing a material balance: where the membrane is assumed to be initially free of adsorbate, V is the liquid volume (assumed to remain constant for dilute feeds) (L), and A is the area of membrane (cm^2), q_e (total MB adsorbed at equilibrium) can be calculated by using following formula.

$$q_e = \frac{(C_0 - C^*)}{(A/V)} \quad \ldots\ldots\ldots\ldots \quad 4$$

The calculated global adsorption kinetic constants, and adsorbed amount (q_e) of corresponding membranes are summarized in Table 4. The highest amount of MB adsorbed on 16mM (7.02 µg/cm^2) at equilibrium (Fig. 13 and Table 4), is due to the increased surface area of TiO_2 nanoparticles deposited on the membrane. The adsorption of MB was increased with TiO_2 loading because of the extra specific surface area of TiO_2 exposed for adsorption. However, in the

case of 32mM, this is not true, and the total amount of adsorbed MB (5.12 µg/cm^2) was even lower than the non-coated membrane (5.89 µg/cm^2). That is probably due to the observed agglomerates of TiO_2 blocking the membrane pores (Fig. 10a,b), and preventing adsorption of MB on PVDF membrane. The quantity of MB adsorbed on 0mM was almost the same as 8mM. Due to the higher adsorption rate for 8mM, adsorption equilibrium reached after 30 min, while for other membranes, equilibrium time was almost 40 min. However, P is the product of surface area (a) and mass transfer coefficient k_L. The point is that when added layer of TiO_2 increases (a increases), the mass transfer resistance increases resulting in a lower value of mass transfer coefficient (k_L). These two opposite effects in the global adsorption kinetic constant (P) could be reason for an unclear trend of the constant as TiO_2 load increases (Table 4)

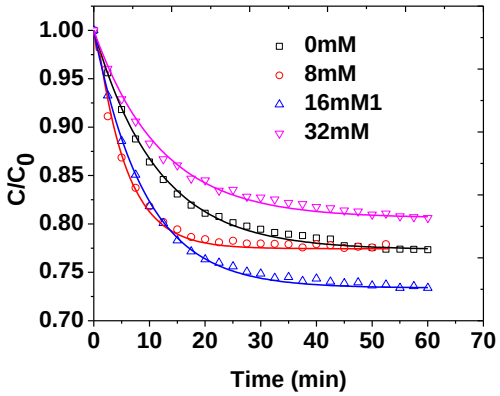

Fig. 13 Rate of adsorption of MB onto 0mM and TiO_2 coated membranes (8mM, 16mM, and 32mM) (Open symbols stand for experimental results, and lines correspond to fitted values)

Table 4 Global adsorption kinetic constant values for adsorption of MB on TiO_2 coated PVDF membranes and amount adsorbed at equilibrium.

Membranes	P (min^{-1}) $= k_L \times a$	Amount adsorbed, q_e, (µg MB/cm^2 membrane)
0mM	0.086	5.89
8mM	0.178	6.09
16mM1	0.106	7.02
32mM	0.082	5.12

We examined the photocatalytic activity of TiO_2 coated PVDF membranes by degrading MB under sunlight with a solar simulator and the experimental results are shown in Fig. 14. After 4 hours of irradiation, non-coated PVDF membrane (0mM) removed 70% of MB due to photosensitization effect of MB. It is reported that under UV light irradiation, C≡N bond of MB, adsorbed on membrane, could be scissor from aromatic ring [24] and results in reduced MB concentration. Additionally, for the same experimental conditions, more than 92% of MB was degraded by 16mM1 membrane, while MB removal was almost 80% in case of 8mM membrane. However, in the case of 32mM membrane, the highest TiO_2 loaded one, the rate of MB degradation is decreased and about 84% of MB removed. The depletion in active surface area due to nanoparticles agglomeration and non-homogeneous distribution of TiO_2 nanoparticles could be the reason for the reduced performance of 32mM.

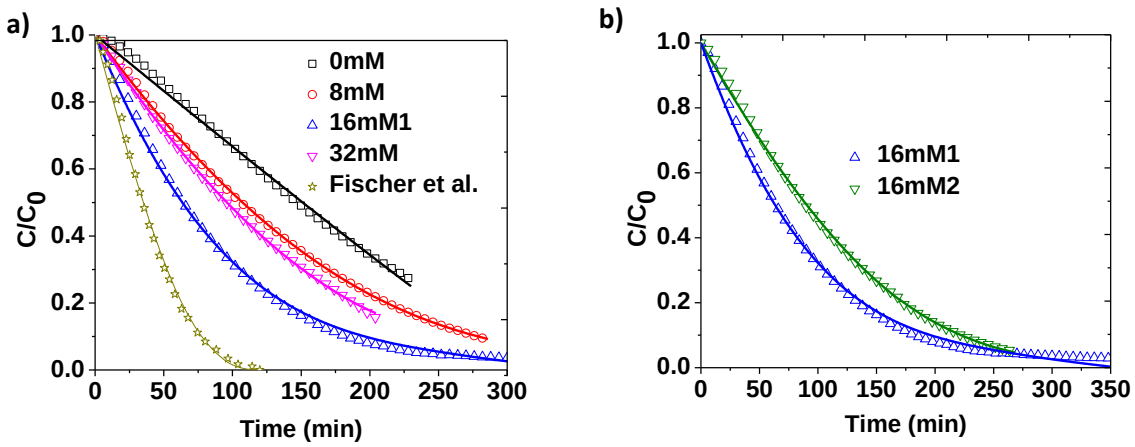

Fig. 14 (a) MB photocatalytic degradation performance as a function of time with pure PVDF (0mM) and TiO_2 coated membranes prepared with different concentration sol-gel solution (8mM, 16mM, and 32mM); (b) Reproducibility test by performing MB photodegradation with two 16mM membranes (16mM1, 16mM2) (Open symbols represent experimental results, and similar color lines stands for the Langmuir-Hinshelwood fitted values)

The photodegradation activity of 16mM1 was highest among all coated membranes (Fig. 14a). Considering this, following the same procedure, we prepared another 16mM (16mM2) PMs to check the reproducibility of the process. Although a similar trend was observed, there was a deviation from one membrane to the other (Fig. 14b). Thus, the sol-gel process requires more experiments to ensure the reproducibility for the preparation of TiO_2 coated PVDF membranes.

We fitted the experimental kinetic data to Langmuir–Hinshelwood model (eq. 1) [54][50][22][45], which is generally used for photocatalytic degradation process (Fig. 14). As we prepared our membranes following Fischer et al. [16], and hence to compare our results, we fitted their MB degradation data to the same mechanism. Since the initial concentration, membrane area and volume treated in the experiment Fischer et al. [16] was different, we also calculated the MB removal rate in terms of µg of MB per hour per cm^2 PMs from 30 minutes and 2 hours degradation results. The following Table 5 summarized the deduced parameters (k_{app}, K_{ads}, k_r) of the Langmuir-Hinshelwood model, % removal of MB after 2 h, and estimated removal rate (µg of MB/h/cm^2 PMs) from 30 min and 2 h degradation result. From Table 5, we notice the highest value of k_{app} for 16mM2 among all membranes, although we observe the best photocatalytic performance for 16mM1 (Fig. 14a,b). The reason is that k_{app} is the product of adsorption constant (K_{ads}) and reaction rate constant (k_r). The adsorption rate of MB on 16mM2 was stronger than 16mM1, while the reaction rate constant was almost one-third of 16mM1. We observed a similar phenomenon for the degradation kinetics from Fischer et al. [16], higher apparent kinetics constant is due to a higher adsorption constant. Moreover, after 2 hours of irradiation, 16mM1 removed the

highest amount of MB (9.81 µg MB/(h×cm^2 PMs)), while least MB degradation was for Fischer et al. [16] (1.55 µg MB/(h×cm^2 PMs)). A similar phenomenon is also observed from 30 min result. Therefore, the photocatalytic performance of our membranes is better than Fischer et al. [16] mentioning that they used a UV- A sunlamp with an intensity of 7.6 mW/cm^2, in our case, it was a solar simulator (sunlight) with 100 mW/cm^2 light intensity.

Table 5 The Langmuir-Hinshelwood parameters for MB photodegradation with removal performance of TiO_2 coated membranes

Membranes	8mM	16mM1	16mM2	32mM	Fischer et al. [16]
k_{app} (min^{-1})	0.012	0.014	0.018	0.014	0.081
K_{ads} (L/mg)	0.24	0.10	0.424	0.248	1.37
k_r (mg/(L×min))	0.051	0.142	0.043	0.056	0.06
% MB removal after 2 hours	55%	76%	65%	60%	100%
µg of MB/ (h×cm^2 PMs) (after 30 min)	7.38	12.5	8.06	8.88	2.83
µg of MB/ (h×cm^2 PMs) (after 2 h)	7.1	9.81	8.39	7.75	1.55

The sol-gel method is easy to deposit TiO_2 nanoparticles on the PVDF membrane from a lower concentration solution. However, preparation of the more photoactive membrane with high TiO_2 content from highly concentrated sol-gel solutions was quite challenging, at least when using TIB as precursor. In the next section, we describe the results with TiO_2/PVDF blended photocatalytic membranes via electrospinning process.

4.2 TiO_2 blended PVDF Electrospun membranes

4.2.1 Surface Morphology of Electrospun membranes

Nano-fibers of pure electrospun PVDF were smooth and more uniform (Fig. 15a,c) and had an average diameter of 108.16 ± 41.19nm (N = 83) (see Annex 10a). After adding TiO_2 and PVP with PVDF polymer and dried, obtained PPTM nanofibers were nonporous or may be microporous with nanoparticles on its surface. There were some clusters of TiO_2 nanoparticles (arrow in Fig. 15d) due to agglomeration. Nanofibers were non-uniform with some bead-like structures. There are two reasons for such beads in a electrospun nano-mat; less viscous polymeric solutions, and lower applied voltage [68]. Lee et al. [36] obtained a bead-free nanomat using the same polymeic solutions but applied +12 kV, whereas we applied +10 kV. During electrospinning, applying a high electric field stretched a charged polymeric jet to form uniform nanofibers; therefore, bead-structures in nano-mat can be avoided by optimizing the applied voltage [68]. The average diameter of these non-porous PPTM nanofibers was 256.83 ± 128.87nm (N = 112), which is almost double than pure PVDF nanofibers (see Annex 10b).

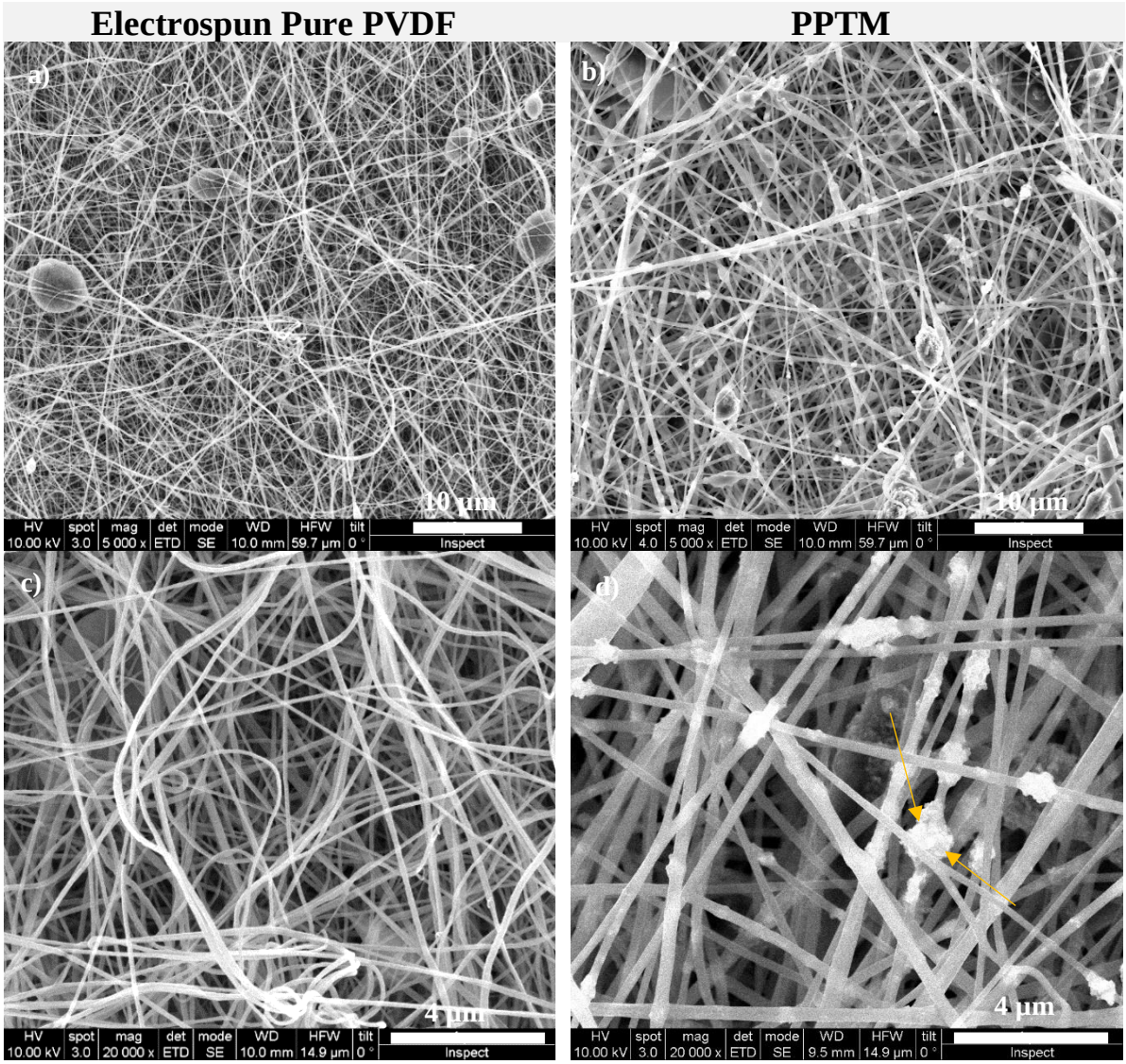

Fig. 15 SEM images of (a, c) electrospun pure PVDF and (b, d) TiO_2 mixed electrospun nanomat before removal of PVP (PPTM) at two different magnifications.

The surface morphology of electrospun PTM nano-mat is shown in Fig. 16. After removing sacrificial PVP, the washed PTM nanofibers had porous and rougher surface (Fig. 16a,b,c) with remaining polymeric beads. The highly porous PTM nanofiber structure provides an advantage in terms of more accessibility to the catalytic TiO_2 to degrade the organic pollutants. Besides, the diameter of porous PTM nanofibers was decreased to an average value of 186.1 ± 69.04 nm (N=117), which is about 0.73 times smaller than the PPTM (see Annex 10c).

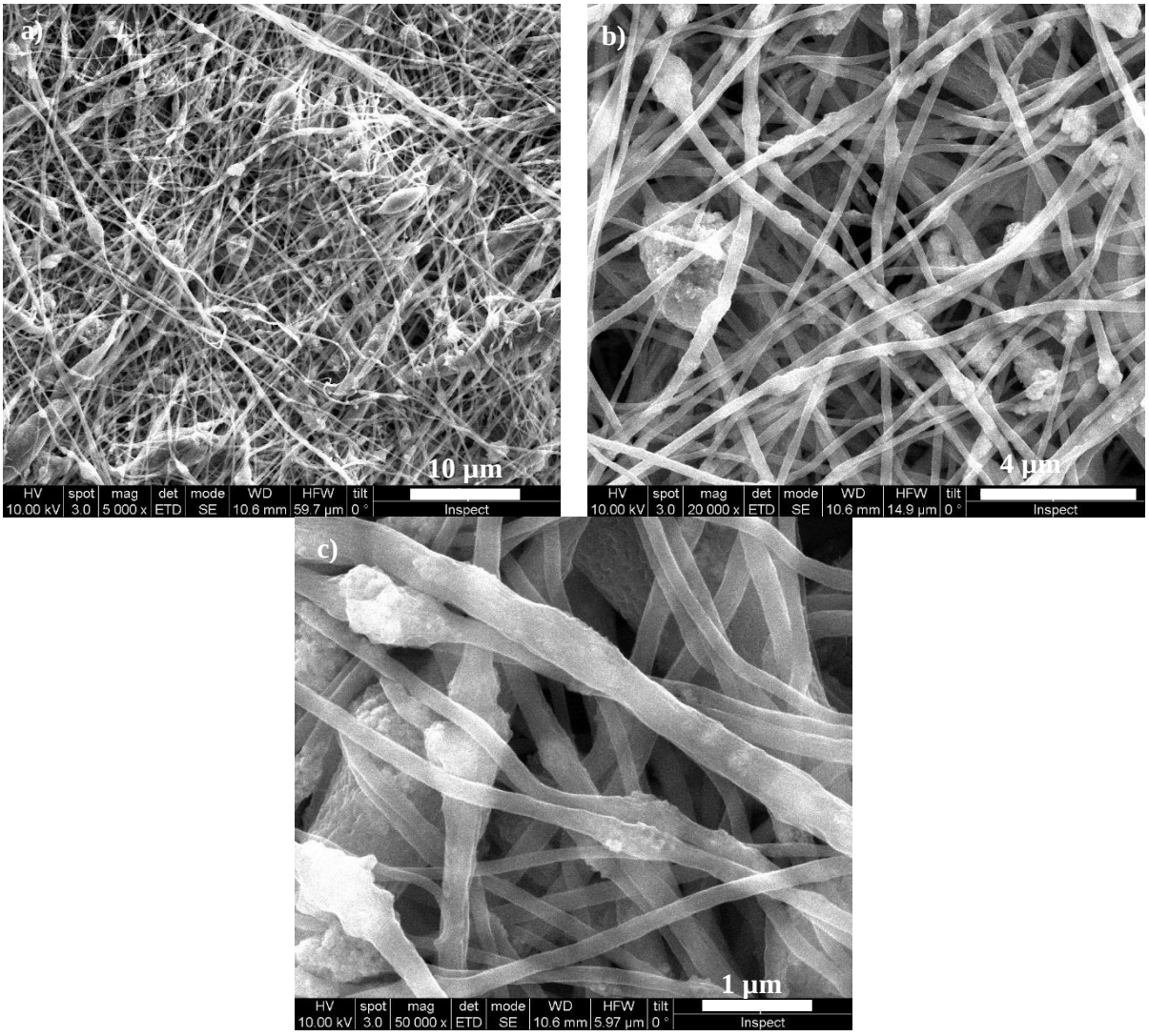

Fig. 16 Surface morphology of PTM, TiO_2 blended PVDF nanomat after removing of sacrificial PVP, and corresponding enlarged images.

4.2.2 Thermogravimetric Analysis of Electrospun membranes

We performed thermogravimetric analysis to evaluate loads of the different polymers and TiO_2 in the final membrane (Fig. 17). For the TGA analysis, we took samples from two different parts (side and middle) of the nano-mat, to identify the distribution of TiO_2 within the nanomat. The decomposition temperature of pure PVDF reported in the literature is 400-450 ˚C [69][70], which agrees with our experimental results, 420 ˚C (Fig. 17). The decomposition of PVDF started at 420 ˚C and finished at 570 ˚C, with the highest decomposition rate at 477 ˚C (Fig. 17). Adding TiO_2 and PVP with PVDF, thermal stability of electrospun PPTM membrane decreases, with an initial decomposition temperature of 290 ˚C and final decomposition temperature of 600 ˚C, which exceeds pure PVDF. The earlier drop in mass loss for PPTM is due to the lower thermal stability

of PVP. The thermal degradation of pure PVP starts at 330 ˚C and finishes at 400 ˚C with the highest decomposition rate at 390 ˚C [71]. In all the TGA of the composite PPTM membranes, before removal of PVP, we observed an instability in the thermobalance maybe because of the high heating ramp in the experiments 10 ºC/min. The experiments should be repeated at a lower heating rate i.e. 2 ºC/min for a better evaluation of the degradation process of the composite membrane.

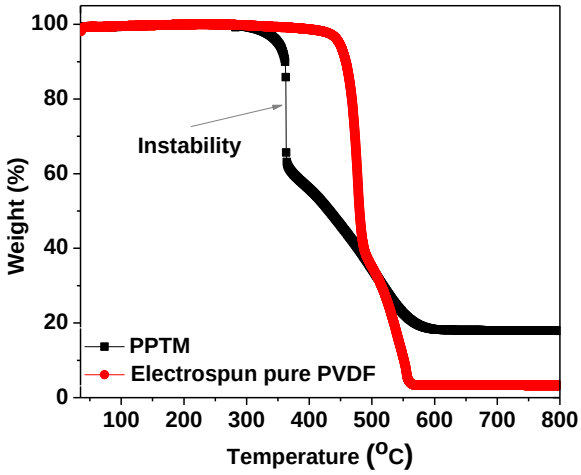

Fig. 17 TGA results of Electrospun Pure PVDF membrane and electrospun PVDF/PVP/ TiO_2 membranes (PPTM), before removal of PVP.

The final remnant of the TGA experiment after 600 ºC signifies the amount of TiO_2 in the corresponding samples. For pure PVDF, we obtained 3.2% of remnant (Fig. 17), which is due to the added LiCl with pure PVDF electrospun solution [65].

4.2.3 Adsorption and Degradation of Methylene Blue

We studied the adsorption rate of MB onto the prepared membranes and fitted the kinetics results to batch adsorption kinetics equation, as same as TiO_2 coated membranes (eq. 3) (Fig. 18). The the global adsorption kinetics constant deduced from the eq. 3, and calculated amount of MB adsorbed on membrane (eq. 4) are summerized in Table 6. From the experimental values in Fig. 18, and calculated amount of MB adsorbed per area of membrane (q_e), non-porous electrospun pure PVDF membrane adsorbed negligible amount (0.69 µg MB/cm^2) of MB and reached equilibrium after 20 minutes only. Meanwhile, porous PTM membranes adsorb almost 25-30 wt% of MB of the solution at equilibrium (Fig. 18), which is an advantage of porous nano-mat. In this case, equilibrium reached after 1 h. However, membrane taken from the middle of nanomat (PTM1, and PTM2), adsorb more MB (7.3 µg MB/cm^2) than PTM3 (taken from the side part of the nanomat), which adsorb 6.54 µg MB/cm^2 of MB. However, the global adsorption kinetic constant shows the

highest value for the PTM3. The possible reason could be the opposite effect of surface area and mass transfer coefficient, and resistance of mass transfer increases due to decrease in mass transfer coefficient.

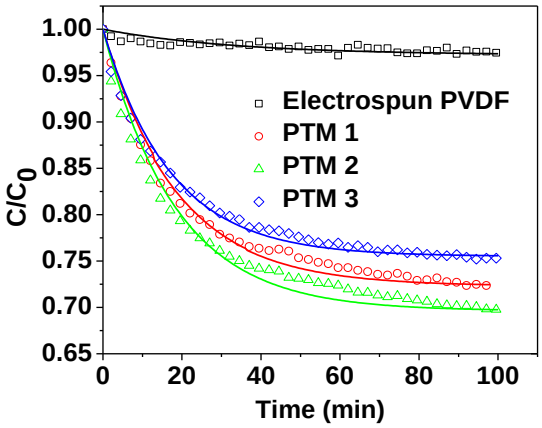

Fig. 18 Rate of Adsorption of MB onto Electrospun PVDF and TiO_2 blended electrospun membranes (PTM1, PTM2, and PTM3; Open symbols stands for experimental values and lines correspond to fitted values

Table 6 Global adsorption kinetic constant values for adsorption of MB on TiO_2 blended electrospun membranes and amount adsorbed at equilibrium

Membranes	P (min^{-1}) $= k_L \times a$	Amount adsorbed, q_e, (µg MB/cm^2 membrane)
Electrospun pure PVDF	0.029	0.69
PTM1	0.052	7.3
PTM2	0.054	7.3
PTM3	0.057	6.54

Once the adsorption-desorption equilibrium was reached, we turned on the solar simulator and the concentration of MB in the solution then decreased faster due to photo-degradation (Fig. 19).

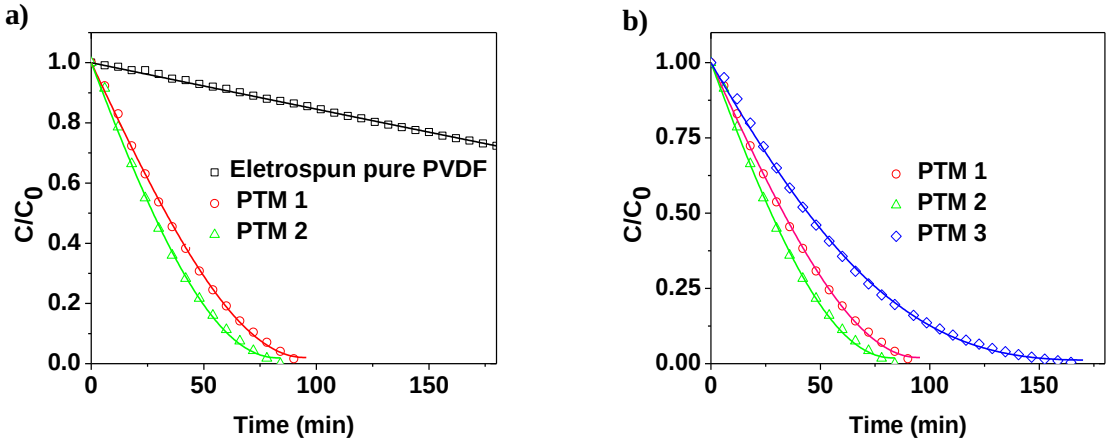

Fig. 19 (a) Photocatalytic degradation performance of MB under UV light as a function of time for electrospun membranes (Electrospun pure PVDF and membrane cut from the middle of TiO_2 /PVDF electrospun nanomat, (PTM1 and PTM2); and (b) Comparison of photocatalytic activity of TiO_2 / PVDF membrane cut from different parts of the nanomat (PTM1, PTM2: mid-portion and PTM3: side-part). (Open symbols refers experimental results and lines denotes Langmuir-Hinshelwood fitted values.

Pure electrospun PVDF removed only 30% of the total MB after 3 hours of irradiation (Fig. 19a), which is almost half of the amount of MB degraded by commercial non-coated PVDF membrane (Fig. 14a). That is because electrospun PVDF adsorbed less amount of MB (Fig. 18), and hence less number of C≡N bond of the aromatic ring of MB had broken during photolysis.

PTM1, and PTM2, membranes taken from the mid-portion of nanomat, decomposed 100% MB after 80 and 90 minutes (Fig. 19a) for the corresponding membranes. Meanwhile, we observed comparatively a slow degradation for PTM3 (cut from the side of nanomat) and after 3 hours of irradiation a complete degradation was observed. This is because less amount of MB adsorbed on the membrane surface (Fig. 18).

We fitted the MB decomposition kinetics results to Langmuir-Hinshelwood mechanism (eq. 1) [54][50][22][45] and summarized the estimated reaction rate parameters, time for 100% removal of MB, and µg of MB removal per hour per area of PMs in Table 7. The highest kinetic constant for PTM1 and PTM3 with the same adsorption constant. However, although the reaction rate constant almost same for PTM1 and PTM3, due to the weak adsorption, PTM3 had the least apparent reaction rate constant.

Table 7 The Langmuir-Hinshelwood parameters for MB photodegradation with removal performance of TiO_2 blended membranes

Membranes	PTM1	PTM2	PTM3	Lee et al. (2mM) [36]
k_{app} (min^{-1})	0.091	0.094	0.04	0.0435 (1st order kinetics)
K_{ads} (L/mg)	1.03	1.01	0.44	-
k_r (mg/(L×min))	0.088	0.093	0.088	-
t_f for 100% MB degradation (min)	90	80	180	90
µg of MB/ (h×cm^2 PMs)	17.21	19.36	8.6	10.66

We followed Lee et al. [36] to prepare electrospun nano-mat, but oven-dried the membrane to remove residual solvent, and then washed out PVP with water, while Lee et al. [36] used a non-solvent (water) induced phase separation (NIPS) method to remove the remaining solvent and PVP. We had almost the same catalyst loading as Lee et al. [36], however, we removed more MB (19.36 µg of MB/(h×cm^2 PMs)) than Lee et al. [36] (10.66 µg of MB/(h×cm^2 PMs) ; thus, photoactivity of our membrane is better than Lee et al. [36]. Nonetheless, we applied different light source than Lee et al. [36], they used six 4W UVA lamps, for photodegradation, and reaction rate depend on the light source, and therefore, our results fitted in Langmuir-Hinshelwood mechanism, it was 1st order for Lee et al. [36].

We also examined the reusability of electrospun nano-mat. Using the same membrane, we performed two more photodegradation experiments (Fig. 20). After each treatment, we wash the membrane with mili-Q water and dried at ambient temperature. However, the photodegradation efficiency of each membrane decreased after every cycle. The loss of efficiency is explained by the washing out of some TiO_2 nanoparticles due to mechanical stirring during the first treatment, and posterior cleaning step.

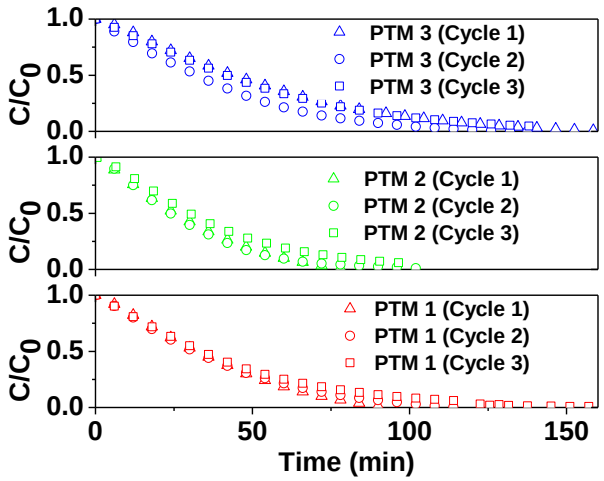

Fig. 20 Reusability of electrospun membranes (PTM1, PTM2, and PTM3)

5. Conclusion

We successfully fabricated TiO_2 coated PVDF membranes by sol-gel method and highly porous TiO_2 blended PVDF nanomat via electrospinning process. We characterized both TiO_2-embedded PVDF membranes and evaluated the photocatalytic performance by degrading MB in a batch reactor. From this study, we can draw the following conclusions.

1. Membrane prepared from 16 mM TIB/Ethanol solution provide better photocatalytic performance. We did not observe any detectable TiO_2 in the membranes prepared from lower concentration (2-4 mM) sol-gel. Meanwhile, it was quite challenging to fabricate a highly photoactive TiO_2-coated PVDF membrane from a concentrated sol-gel solution. Because, higher concentration sol-gel solution yields agglomeration and non-homogeneous distribution of TiO_2 nanoparticles, which blocks the membrane pores. The addition of a stabilizing agent in an acidic sol-gel could solve this problem.
2. The TiO_2-embedded highly porous electrospun nano-mat shows an excellent photoactivity towards MB degradation. Under solar irradiation, we decomposed 100% of MB within 80 min. Therefore, this porous TiO_2-anchored PVDF fiber mat can be a solution to dye contaminated wastewater problems. Additionally, using this method, we can anchor visible-light responsive modified-TiO_2 to fabricate highly porous visible-light-driven photocatalytic membranes, which can be used in energy-saving and practical applications.

References

[1] P. Kumari, N. Bahadur, and L. F. Dumée, "Photo-catalytic membrane reactors for the remediation of persistent organic pollutants – A review," *Sep. Purif. Technol.*, vol. 230, no. May 2019, p. 115878, 2020.

[2] G. Matafonova and V. Batoev, "Recent advances in application of UV light-emitting diodes for degrading organic pollutants in water through advanced oxidation processes: A review," *Water Res.*, vol. 132, pp. 177–189, 2018.

[3] S. K. Loeb *et al.*, "The Technology Horizon for Photocatalytic Water Treatment: Sunrise or Sunset?," *Environ. Sci. Technol.*, vol. 53, no. 6, pp. 2937–2947, 2019.

[4] T. Van Gerven, G. Mul, J. Moulijn, and A. Stankiewicz, "A review of intensification of photocatalytic processes," *Chem. Eng. Process. Process Intensif.*, vol. 46, no. 9 SPEC. ISS., pp. 781–789, 2007.

[5] S. Mozia, "Photocatalytic membrane reactors (PMRs) in water and wastewater treatment. A review," *Sep. Purif. Technol.*, vol. 73, no. 2, pp. 71–91, 2010.

[6] O. Iglesias, M. J. Rivero, A. M. Urtiaga, and I. Ortiz, "Membrane-based photocatalytic systems for process intensification," *Chem. Eng. J.*, vol. 305, pp. 136–148, 2016.

[7] K. C. Lee and K. H. Choo, "Optimization of flocculation conditions for the separation of TiO_2 particles in coagulation-photocatalysis hybrid water treatment," *Chem. Eng. Process. Process Intensif.*, vol. 78, pp. 11–16, 2014.

[8] J. C. Espíndola, R. O. Cristóvão, A. Mendes, R. A. R. Boaventura, and V. J. P. Vilar, "Photocatalytic membrane reactor performance towards oxytetracycline removal from synthetic and real matrices: Suspended vs immobilized TiO_2-P25," *Chem. Eng. J.*, vol. 378, no. April, p. 122114, 2019.

[9] R. L. Fernández, J. A. McDonald, S. J. Khan, and P. Le-Clech, "Removal of pharmaceuticals and endocrine disrupting chemicals by a submerged membrane photocatalysis reactor (MPR)," *Sep. Purif. Technol.*, vol. 127, pp. 131–139, 2014.

[10] S. Singh, H. Mahalingam, and P. K. Singh, "Polymer-supported titanium dioxide photocatalysts for environmental remediation: A review," *Appl. Catal. A Gen.*, vol. 462–463, pp. 178–195, 2013.

[11] Y. Shi, J. Huang, G. Zeng, W. Cheng, and J. Hu, "Photocatalytic membrane in water purification: is it stepping closer to be driven by visible light?," *J. Memb. Sci.*, vol. 584, no. May, pp. 364–392, 2019.

[12] S. Leong, A. Razmjou, K. Wang, K. Hapgood, X. Zhang, and H. Wang, "TiO_2 based photocatalytic membranes: A review," *J. Memb. Sci.*, vol. 472, pp. 167–184, 2014.

[13] C. Zhang, M. Huang, L. Meng, B. Li, and T. Cai, "Electrospun polysulfone (PSf)/titanium dioxide (TiO_2) nanocomposite fibers as substrates to prepare thin film forward osmosis membranes," *J. Chem. Technol. Biotechnol.*, vol. 92, no. 8, pp. 2090–2097, 2017.

[14] E. Boyraz, F. Yalcinkaya, J. Hruza, and J. Maryska, "Surface-modified nanofibrous PVDF membranes for liquid separation technology," *Materials (Basel).*, vol. 12, no. 7, pp. 1–12, 2019.

[15] J. Hou, G. Dong, Y. Ye, and V. Chen, "Enzymatic degradation of bisphenol-A with immobilized laccase on TiO_2 sol-gel coated PVDF membrane," *J. Memb. Sci.*, vol. 469, pp. 19–30, 2014.

[16] K. Fischer, M. Grimm, J. Meyers, C. Dietrich, R. Gläser, and A. Schulze, "Photoactive microfiltration membranes via directed synthesis of TiO_2 nanoparticles on the polymer surface for removal of drugs from water," *J. Memb. Sci.*, vol. 478, pp. 49–57, 2015.

[17] S. J. You, G. U. Semblante, S. C. Lu, R. A. Damodar, and T. C. Wei, "Evaluation of the antifouling and photocatalytic properties of poly(vinylidene fluoride) plasma-grafted poly(acrylic acid) membrane with self-assembled TiO_2," *J. Hazard. Mater.*, vol. 237–238, pp. 10–19, 2012.

[18] G. De Filpo *et al.*, "Chemical vapor deposition of photocatalyst nanoparticles on PVDF membranes for advanced oxidation processes," *Membranes (Basel).*, vol. 8, no. 3, 2018.

[19] A. Qin, X. Li, X. Zhao, D. Liu, and C. He, "Engineering a highly hydrophilic PVDF membrane via binding TiO_2 nanoparticles and a PVA layer onto a membrane surface," *ACS*

Appl. Mater. Interfaces, vol. 7, no. 16, pp. 8427–8436, 2015.

[20] S. Ren, C. Boo, N. Guo, S. Wang, M. Elimelech, and Y. Wang, "Photocatalytic Reactive Ultrafiltration Membrane for Removal of Antibiotic Resistant Bacteria and Antibiotic Resistance Genes from Wastewater Effluent," *Environ. Sci. Technol.*, vol. 52, no. 15, pp. 8666–8673, 2018.

[21] P. M. Martins, R. Miranda, J. Marques, C. J. Tavares, G. Botelho, and S. Lanceros-Mendez, "Comparative efficiency of TiO_2 nanoparticles in suspension vs. immobilization into P(VDF-TrFE) porous membranes," *RSC Adv.*, vol. 6, no. 15, pp. 12708–12716, 2016.

[22] O. Benhabiles, F. Galiano, T. Marino, H. Mahmoudi, H. Lounici, and A. Figoli, "Preparation and characterization of TiO_2 -PVDF/PMMA blend membranes using an alternative non-toxic solvent for UF/MF and photocatalytic application," *Molecules*, vol. 24, no. 4, pp. 1–20, 2019.

[23] F. Galiano *et al.*, "Novel photocatalytic PVDF/Nano-TiO_2 hollow fibers for Environmental remediation," *Polymers (Basel).*, vol. 10, no. 10, pp. 1–20, 2018.

[24] H. P. Ngang, B. S. Ooi, A. L. Ahmad, and S. O. Lai, "Preparation of PVDF-TiO_2 mixed-matrix membrane and its evaluation on dye adsorption and UV-cleaning properties," *Chem. Eng. J.*, vol. 197, pp. 359–367, 2012.

[25] N. Abdullah, B. V. Ayodele, W. N. W. Mansor, and S. Abdullah, "Effect of incorporating TiO_2 photocatalyst in PVDF hollow fibre membrane for photo-assisted degradation of methylene blue," *Bull. Chem. React. Eng. Catal.*, vol. 13, no. 3, pp. 588–591, 2018.

[26] H. Dzinun *et al.*, "Antifouling behavior and separation performance of immobilized TiO_2 in dual layer hollow fiber membranes," *Polym. Eng. Sci.*, vol. 58, no. 9, pp. 1636–1643, 2018.

[27] O. Tahiri Alaoui, Q. T. Nguyen, C. Mbareck, and T. Rhlalou, "Elaboration and study of poly(vinylidene fluoride)-anatase TiO_2 composite membranes in photocatalytic degradation of dyes," *Appl. Catal. A Gen.*, vol. 358, no. 1, pp. 13–20, 2009.

[28] S. J. You, G. U. Semblante, S. C. Lu, R. A. Damodar, and T. C. Wei, "Evaluation of the antifouling and photocatalytic properties of poly(vinylidene fluoride) plasma-grafted poly(acrylic acid) membrane with self-assembled TiO_2," *J. Hazard. Mater.*, vol. 237–238,

pp. 10–19, 2012.

[29] M. Tavakolmoghadam, T. Mohammadi, M. Hemmati, and F. Naeimpour, “Surface modification of PVDF membranes by sputtered TiO_2: fouling reduction potential in membrane bioreactors,” *Desalin. Water Treat.*, vol. 57, no. 8, pp. 3328–3338, 2016.

[30] Y. Liang, S. Sun, T. Deng, H. Ding, W. Chen, and Y. Chen, “The preparation of TiO_2 film by the sol-gel method and evaluation of its self-cleaning property,” *Materials (Basel).*, vol. 11, no. 3, 2018.

[31] M. E. Simonsen and E. G. Søgaard, “Sol-gel reactions of titanium alkoxides and water: Influence of pH and alkoxy group on cluster formation and properties of the resulting products,” *J. Sol-Gel Sci. Technol.*, vol. 53, no. 3, pp. 485–497, 2010.

[32] H. Rawindran *et al.*, “Simultaneous separation and degradation of surfactants laden in produced water using PVDF/TiO_2 photocatalytic membrane,” *J. Clean. Prod.*, vol. 221, pp. 490–501, 2019.

[33] L. Aoudjit, P. M. Martins, F. Madjene, D. Y. Petrovykh, and S. Lanceros-Mendez, “Photocatalytic reusable membranes for the effective degradation of tartrazine with a solar photoreactor,” *J. Hazard. Mater.*, vol. 344, pp. 408–416, 2018.

[34] P. Dong, Z. Huang, X. Nie, X. Cheng, Z. Jin, and X. Zhang, “Plasma enhanced decoration of nc-TiO_2 on electrospun PVDF fibers for photocatalytic application,” *Mater. Res. Bull.*, vol. 111, no. September 2018, pp. 102–112, 2019.

[35] A. Weijia, X. Ziyi, S. Huaxu, L. Lei, and M. Yefan, “Flexible TiO_2/PVDF/g-C_3N_4 Nanocomposite with Excellent Light Photocatalytic Performance,” no. 2, pp. 81–85, 2018.

[36] C. G. Lee *et al.*, “Porous Electrospun Fibers Embedding TiO_2 for Adsorption and Photocatalytic Degradation of Water Pollutants,” *Environ. Sci. Technol.*, vol. 52, no. 7, pp. 4285–4293, 2018.

[37] H. Salazar *et al.*, “Photocatalytic and antimicrobial multifunctional nanocomposite membranes for emerging pollutants water treatment applications,” *Chemosphere*, vol. 250, 2020.

[38] N. Hoogesteijn Von Reitzenstein, X. Bi, Y. Yang, K. Hristovski, and P. Westerhoff, "Morphology, structure, and properties of metal oxide/polymer nanocomposite electrospun mats," *J. Appl. Polym. Sci.*, vol. 133, no. 33, pp. 1–9, 2016.

[39] C. Ding, H. Fang, G. Duan, Y. Zou, S. Chen, and H. Hou, "Investigating the draw ratio and velocity of an electrically charged liquid jet during electrospinning," *RSC Adv.*, vol. 9, no. 24, pp. 13608–13613, 2019.

[40] D. Lolla, M. Lolla, A. Abutaleb, H. U. Shin, D. H. Reneker, and G. G. Chase, "Fabrication, polarization of electrospun polyvinylidene fluoride electret fibers and effect on capturing nanoscale solid aerosols," *Materials (Basel).*, vol. 9, no. 8, 2016.

[41] L. Paredes *et al.*, "Application of immobilized TiO_2 on PVDF dual layer hollow fibre membrane to improve the photocatalytic removal of pharmaceuticals in different water matrices," *Appl. Catal. B Environ.*, vol. 240, pp. 9–18, 2019.

[42] H. Dzinun *et al.*, "Antifouling Behavior and Separation Performance of Immobilized TiO_2 in Dual Layer Hollow Fiber Membranes," pp. 1–8, 2017.

[43] H. Song, J. Shao, J. Wang, and X. Zhong, "The removal of natural organic matter with LiCl-TiO_2-doped PVDF membranes by integration of ultrafiltration with photocatalysis," *Desalination*, vol. 344, pp. 412–421, 2014.

[44] A. Zhou *et al.*, "Abatement of sulfadiazine in water under a modified ultrafiltration membrane (PVDF-PVP-TiO_2-dopamine) filtration-photocatalysis system," *Sep. Purif. Technol.*, vol. 234, no. 1000, pp. 1321–1328, 2020.

[45] X. Zheng, Z. P. Shen, L. Shi, R. Cheng, and D. H. Yuan, "Photocatalytic membrane reactors (PMRs) in water treatment: Configurations and influencing factors," *Catalysts*, vol. 7, no. 8, 2017.

[46] P. Argurio, E. Fontananova, R. Molinari, and E. Drioli, "Photocatalytic membranes in photocatalytic membrane reactors," *Processes*, vol. 6, no. 9, 2018.

[47] A. J. Karabelas, K. V. Plakas, and V. C. Sarasidis, "How Far Are We From Large-Scale PMR Applications?," in *Current Trends and Future Developments on (Bio-) Membranes: Photocatalytic Membranes and Photocatalytic Membrane Reactors*, 2018, pp. 233–295.

[48] H. C. Aran, D. Salamon, T. Rijnaarts, G. Mul, M. Wessling, and R. G. H. Lammertink, "Porous Photocatalytic Membrane Microreactor (P2M2): A new reactor concept for photochemistry," *J. Photochem. Photobiol. A Chem.*, vol. 225, no. 1, pp. 36–41, 2011.

[49] S. Riaz and S. J. Park, "An overview of TiO_2-based photocatalytic membrane reactors for water and wastewater treatments," *J. Ind. Eng. Chem.*, vol. 84, pp. 23–41, 2020.

[50] D. F. Ollis, E. Pelizzetti, and N. Serpone, "Destruction of water contaminants," *Environ. Sci. Technol.*, vol. 25, no. 9, pp. 1522–1529, 1991.

[51] L. Penboon, A. Khrueakham, and S. Sairiam, "TiO_2 coated on PVDF membrane for dye wastewater treatment by a photocatalytic membrane," *Water Sci. Technol.*, vol. 79, no. 5, pp. 958–966, 2019.

[52] Y. Peng, Z. Yu, Y. Pan, and G. Zeng, "Antibacterial photocatalytic self-cleaning poly(vinylidene fluoride) membrane for dye wastewater treatment," *Polym. Adv. Technol.*, vol. 29, no. 1, pp. 254–262, 2018.

[53] M. N. Subramaniam, P. S. Goh, W. J. Lau, B. C. Ng, and A. F. Ismail, "AT-POME colour removal through photocatalytic submerged filtration using antifouling PVDF-TNT nanocomposite membrane," *Sep. Purif. Technol.*, vol. 191, pp. 266–275, 2018.

[54] W. Z. Tang and Huren An, "UV/TiO_2 photocatalytic oxidation of commercial dyes in aqueous solutions," *Chemosphere*, vol. 31, no. 9, pp. 4157–4170, 1995.

[55] R. Kamaludin, A. S. Mohamad Puad, M. H. D. Othman, S. H. S. A. Kadir, and Z. Harun, "Incorporation of N-doped TiO_2 into dual layer hollow fiber (DLHF) membrane for visible light-driven photocatalytic removal of reactive black 5," *Polym. Test.*, vol. 78, no. June, 2019.

[56] W. Wang, M. O. Tadé, and Z. Shao, "Nitrogen-doped simple and complex oxides for photocatalysis: A review," *Prog. Mater. Sci.*, vol. 92, pp. 33–63, 2018.

[57] N. Li *et al.*, "Precisely-controlled modification of PVDF membranes with 3D TiO_2/ZnO nanolayer: enhanced anti-fouling performance by changing hydrophilicity and photocatalysis under visible light irradiation," *J. Memb. Sci.*, vol. 528, no. 73, pp. 359–368, 2017.

[58] Q. Chen *et al.*, "A novel photocatalytic membrane decorated with RGO-Ag-TiO_2 for dye degradation and oil–water emulsion separation," *J. Chem. Technol. Biotechnol.*, vol. 93, no. 3, pp. 761–775, 2018.

[59] Q. Chen *et al.*, "Enhancing the photocatalytic and antibacterial property of polyvinylidene fluoride membrane by blending Ag–TiO_2 nanocomposites," *J. Mater. Sci. Mater. Electron.*, vol. 28, no. 4, pp. 3865–3874, 2017.

[60] S. Yu, Y. Wang, F. Sun, R. Wang, and Y. Zhou, "Novel mpg-C_3N_4/TiO_2 nanocomposite photocatalytic membrane reactor for sulfamethoxazole photodegradation," *Chem. Eng. J.*, vol. 337, pp. 183–192, 2018.

[61] A. T. Kuvarega, N. Khumalo, D. Dlamini, and B. B. Mamba, "Polysulfone/N,Pd co-doped TiO_2 composite membranes for photocatalytic dye degradation," *Sep. Purif. Technol.*, vol. 191, no. April 2017, pp. 122–133, 2018.

[62] H. H. Mungondori, L. Tichagwa, D. M. Katwire, and O. Aoyi, "Preparation of photo-catalytic copolymer grafted asymmetric membranes (N-TiO_2-PMAA-g-PVDF/PAN) and their application on the degradation of bentazon in water," *Iran. Polym. J. (English Ed.*, vol. 25, no. 2, pp. 135–144, 2016.

[63] H. Xu, M. Ding, W. Chen, Y. Li, and K. Wang, "Nitrogen–doped GO/TiO_2 nanocomposite ultrafiltration membranes for improved photocatalytic performance," *Sep. Purif. Technol.*, vol. 195, no. July 2017, pp. 70–82, 2018.

[64] O. Tahiri Alaoui, Q. T. Nguyen, C. Mbareck, and T. Rhlalou, "Elaboration and study of poly(vinylidene fluoride)-anatase TiO_2 composite membranes in photocatalytic degradation of dyes," *Appl. Catal. A Gen.*, vol. 358, no. 1, pp. 13–20, 2009.

[65] S. Santoro *et al.*, "Experimental evaluation of the thermal polarization in direct contact membrane distillation using electrospun nanofiber membranes doped with molecular probes," *Molecules*, vol. 24, no. 3, 2019.

[66] M. L. Addonizio, A. Aronne, and C. Imparato, "Amorphous hybrid TiO_2 thin films: The role of organic ligands and UV irradiation," *Appl. Surf. Sci.*, vol. 502, no. May 2019, 2020.

[67] K. Assaker *et al.*, "Water-catalyzed low-temperature transformation from amorphous to

semi-crystalline phase of ordered mesoporous titania framework," *ACS Sustain. Chem. Eng.*, vol. 2, no. 2, pp. 120–125, 2014.

[68] M. Rasouli, S. Pirsalami, and S. M. Zebarjad, "Optimizing the electrospinning conditions of polysulfone membranes for water microfiltration applications," *Polym. Int.*, vol. 68, no. 9, pp. 1610–1617, 2019.

[69] P. F. R. Ortega, J. P. C. Trigueiro, G. G. Silva, and R. L. Lavall, "Improving supercapacitor capacitance by using a novel gel nanocomposite polymer electrolyte based on nanostructured SiO_2, PVDF and imidazolium ionic liquid," *Electrochim. Acta*, vol. 188, pp. 809–817, 2016.

[70] A. Jabbarnia, W. S. Khan, A. Ghazinezami, and R. Asmatulu, "Investigating the thermal, mechanical, and electrochemical properties of PVdF/PVP nanofibrous membranes for supercapacitor applications," *J. Appl. Polym. Sci.*, vol. 133, no. 30, pp. 1–10, 2016.

[71] A. F. Basha and M. A. F. Basha, "Structural and thermal degradation studies on thin films of the nanocomposite system PVP-$Ce(SO_4)24H_2O$," *Polym. Bull.*, vol. 68, no. 1, pp. 151–165, 2012.

[72] S. Sakarkar, S. Muthukumaran, and V. Jegatheesan, "Evaluation of polyvinyl alcohol (PVA) loading in the PVA/titanium dioxide (TiO_2) thin film coating on polyvinylidene fluoride (PVDF) membrane for the removal of textile dyes," *Chemosphere*, vol. 257, 2020.

[73] Z. Xu *et al.*, "Photocatalytic antifouling PVDF ultrafiltration membranes based on synergy of graphene oxide and TiO_2 for water treatment," *J. Memb. Sci.*, vol. 520, pp. 281–293, 2016.

[74] L. A. Shah, T. Malik, M. Siddiq, A. Haleem, M. Sayed, and A. Naeem, "TiO_2 nanotubes doped poly(vinylidene fluoride) polymer membranes (PVDF/TNT) for efficient photocatalytic degradation of brilliant green dye," *J. Environ. Chem. Eng.*, vol. 7, no. 5, 2019.

[75] O. Benhabiles, F. Galiano, T. Marino, H. Mahmoudi, H. Lounici, and A. Figoli, "Preparation and characterization of TiO_2-PVDF/PMMA blend membranes using an alternative non-toxic solvent for UF/MF and photocatalytic application," *Molecules*, vol. 24, no. 4, pp. 1–20, 2019.

[76] J. Sun, S. Li, Z. Ran, and Y. Xiang, "Preparation of Fe_3O_4@TiO_2 blended PVDF membrane by magnetic coagulation bath and its permeability and pollution resistance," *J. Mater. Res. Technol.*, vol. 9, no. 3, pp. 4951–4967, 2020.

[77] R. Kamaludin *et al.*, "Visible-light active photocatalytic dual layer hollow fiber (DLHF) membrane and its potential in mitigating the detrimental effects of bisphenol A in water," *Membranes (Basel).*, vol. 10, no. 2, 2020.

[78] Q. Wang, C. Yang, G. Zhang, L. Hu, and P. Wang, "Photocatalytic Fe-doped TiO_2/PSF composite UF membranes: Characterization and performance on BPA removal under visible-light irradiation," *Chem. Eng. J.*, vol. 319, pp. 39–47, 2017.

[79] H. Zangeneh, A. A. Zinatizadeh, and S. Zinadini, "Self-cleaning properties of L-Histidine doped TiO_2-CdS/PES nanocomposite membrane: Fabrication, characterization and performance," *Sep. Purif. Technol.*, vol. 240, 2020.

Appendices

Annex 1 List of Abbreviations and Symbols

Polymers

PVA	Polyvinyl alcohol
PAA	Poly(acrylic acid)
P(VDF-TrFE)	Poly(vinylidenefluoride-co-trifluoroethylene)
PEG	Poly (ethylene glycol)
PVDF	Poly(vinylidene fluoride)
PMMA	Poly (methylmethacrylate)
PDA	Polydopamine
PES	Polyethersulfone
PSf	Polysulfone
DA	Dopamine
PEGMA	Poly(ethylene glycol) methyl ether methacrylate
CA	Cellulose Acetate

Pollutant

MB	Methylene Blue
IBPR	Ibuprofen
DS	Dichlofenac Sodium
MO	Methyl Orange
RB	Reactive Blue
RdB	Rodamine B
RB5	Reactive black 5
BSA	Bovine Serum Albumin
BG	Brilliant green
BPA	Bisphenol A
EE2	17α-ethynylestradiol
HA	Humic Acid
POME	Palm oil mill effluent
NP	Nonylphenol
Tartz	Tartzarine
SULF	Sulfadiazine
Ind. Surf	Industrial Surfactant
EY	Eosin Yellow
SFMO	Sulfamethoxazole
Bentz	Bentazon

Solvent and other additives

NMP	1-Methyl-2-pyrrolidone
DMF	N,N-dimethylformamide
mpg-C_3N_4	Mesoporous graphitic carbon nitride
DMAc	N,N- dimethyl acetamide
TTIP	Titanium tetraisopropoxide
EtOH	Ethanol
APTES	Aminopropyltriethoxysilane
TEP	triethyl phosphate
RGO	Reduced Graphene Oxide
GLUT	Glutaraldehyde

Others

HF	Hollow Fiber
DHLF	Dual Layer Hollow Fiber Membrane
N.D.	Not Detectable
ALD	Atomic Layer Deposition

List of Symbols

θ	Contact Angle
ε	Porosity
Model	Model pollutant
V_0	Volume of contaminated solution
C_0	Initial concentration
D	Degradation
R	Rejection
k_{app}	Apparent reaction kinetic constant
A	Area of the membrane
I	Irradiation source and power
t	Total irradiation time
P	Performance in terms of µg of pollutant removed per hour per area of PMs
υ	Recirculation velocity

Annex 2 UV-responsive PMs used in different types of PMRs, their Photocatalytic Activity and other membrane performances with operating conditions

Annex 3 Batch PMRs Using Flat Sheet PMs

PM type	wt% TiO_2 added	θ (°)		ε (%)		M	C_0 , V_0, pH,	I, t, A	D (%)	k_{app} (min^{-1})	P (μg/(h× cm^2))	Observation and other performances	Ref.
		PVDF	PM	PVDF	PM								
TiO_2/PVDF(2 mM TTIP/ EtOH sol-gel)	0.092 wt% of dry PMs	73	76	7% of porosity reduced		MB	3.2 mg/L, 4 mL	76 W/m^2 UV-A, 2.5 h, 4.12 cm^2.	100% (2 h)		1.55	Decrease hydrophlicity and porosityof PMs and hence water flux decreased but BSA filtration performance improved	[16]
						IBRF	100 mg/L, 4 mL		45 %		48.5		
						DS	25 mg/L, 4 mL		70%		12.13		
PVA/TiO_2/PVDF	1%	87	59	44	38	RB	50 mg/L, 150 ml	15W UV-C lamp, 2.5 h, 25 cm^2	44%	-	26.4	At optimum PVA (3 wt%) and 1 wt% TiO_2 improved mechanical property and hydrophilicty but above this value TiO_2 encapsulate.	[72]
						RdB			45%	-	27		
						MO			48%	-	28.8		
TiO_2/PAA/PVDF	0.5 (w/v)	116	28			RB5	40 mg/L, 25mL	15W UV lamp, 2 h, 25 cm^2	30%	0.031	6	Higher flux obtained under UV due to high antifouling property of the membrane. 3 wt% loading of TiO_2 shows best photocatalytic activity.	[28]
	1. 5 (w/v)		23						30%	0.033	6		
	3 (w/v)		N.D						42%	0.042	8		
TiO_2/PVP/PVDF/DMAc	1%	79	65	70	75	BSA	1000 mg/L, 50 mL.	11W UV, 2 h, 19.3 cm^2	53%	0.0068	686.5	Addition of TiO_2 decrease surface roughness, and incorporation GO faster the photodegradation of BSA and improve the BSA rejection and water flux.	[73]
GO/TiO_2/PVP/PVDF/DMAc	1%		61	70	83				80%	0.0142	1036.3		
TiO_2 nanotube/ PVP/PVDF/ DMAc	0.1%	92	82	28	43	BG	150 mL. pH 7.5,	15W Hg-lamp, 1.5 h, 50 cm^2.	42% for 1.5 wt%			Best antifouling property obtained for 1.5 wt% TiO_2 content, more than this porosity, mechanical stability and water flux decreased.	[74]
	0.5%		-		47								
	1.0%		73		50								
	1.5%		70		56								
	2%		-		36								
TiO_2/P(VDF–TrFE)/ DMF	3%	76	88	80	78	MB	3.2 mg/L, 13 mL, pH 6.8	40 W/m^2 LED UVA, 1.5 h, 12 cm^2	77%	0.018	1.78	8 wt% TiO_2 shows better photodegradation but porosity and hydrophilicity decreased. Inclusion of a zeolite (NaY) can increase hydrophilicity and porosity by aiding microporosity and capillary effect of zeolite.	[21]
	5%		97		77				93%	0.026	2.15		
	8%		97		74				99%	0.037	2.29		
NaY/TiO_2/P(VDF-TrFE) /DMF	3% NaY		N.D		90				91%	0.023	2.1		
	5% NaY				95				99%	0.04	2.29		
	8% NaY				97				96%	0.033	2.22		
TiO_2/PVDF/PMMA/PEG/PVP/TEP	0.12 %	110	102	82	80	MB	3.2 mg/L, 500 mL	500W UV lamp, 6.5 h, 16 cm^2	86%	0.0055	10.58	TiO_2 loading increase the porosity, hydrophilicity, and mechanical properties of PMs.	[75]
	0.25%		98		81				95%	0.0084	11.69		
	0.50%		93		83				99%	0.0117	12.18		
TiO_2/PVDF/PVP/DMAc	4%	108	61			MB	6.4 mg/L, 50 mL	UVA lamp 4W, 1.5 h, 20 cm^2	100 %	0.044	10.66	Fabrication of highly porous and photoactive PMs using a bipolymer system through electrospinning process.	[36]
						BPA	5.0 mg/L, 50 mL		96% (4 h)	0.030	3		
						EE2	5.0 mg/L, 50 mL		96%	0.033	8		

Annex 4 Continuous PMRs Using Flat Sheet PMs

Flat sheet (Dead End)

PM type	wt% TiO_2 added	θ (°) PVDF	θ (°) PM	ε (%) PVDF	ε (%) PM	M	C_0 , V_0, pH, υ	I, t, A	D (%) or R (%)	k_{app} (min^{-1})	Observation and other performances	Ref.
TiO_2/PVDF/H_2O	0.1 g/L**	128	127	75	34	RB 19	25 mg/L, pH 3, 0.877 L/min	9W UV-C, 1 h, 59.5 cm^2.	19%		Negatively charged RB5 favors acidic pH, alkaline condition decreases photoactivity.	[51]
	0.5 g/L		121		39				26%			
	1 g/L		114		40				35%			
TiO_2/PDA/PVDF	1.5 %	85	65	14	8	ARB	10 mL (cell)	0.12 W/m^2 UV lamp, 3 h, 4.1cm^2	98%		Increased hydrophilicity, and high antifouling properties	[20]
						ARGs			98%			
Flat sheet (Cross flow)												
TiO_2/PVDF (CVD)	-	61 90	26	70	-	MB	4.15 mg/L	6 W/m^2 Hg-lamp, 6 h, 14.5 cm^2	92% (4 h)	0.028	Needed to optimize sputtering conditions. Increased in hydrophilicity improved transmembrane fluxes.	[18]
						DS	29.6 mg/L, 250 mL/min		100%	0.0083		
TiO_2/PVP/PVDF/ DA/DMAc	0.8%	80	30			SULF	100 µg/L, 100 mL. pH 7.5, 30 L/h	1.25 W/m^2 UV, 2 h, 26.12 cm^2.	91.4%	0.0216	Rejection increased under UV irradiation because of synergistic effect of photodegradation and filtration.	[44]
TiO_2/LiCl/PVDF/ DMAc	0.5%		75			HA	2 mg/L, pH 7.5, 500 mL/min	100 W Hg-lamp, 8 h, 48 cm^2	82% of R		Better NOM rejection and reduction of membrane fouling with good self-cleaning ability.	[43]
Fe_3O_4@TiO_2/PV DF/NMP	0.5%	A decrease of 10° for PMs		1.5	1.6	HA	20 mg/L, 100 mL. pH 7.5, 100 L/h	19W Hg-lamp, 2 h, 50 cm^2.	67% of R		Most of the nanoparticles flocculate on the surface of PMs because of magnetic coagulation bath. Under UV, PMs had better antifouling performance against humic acid solution.	[76]
	1%				1.7				69% of R			
HF (Cross flow)												
TiO_2/PVP/PVDF/ NMP	0.5%	88	78	36	40	Ind. Surf.	COD ~1420 mg/L, pH 6.8, 410 mL/min	8 W UV-A, 36 cm^2	66.7% of R		Under UV-light optimum content of TiO_2 (2 wt%) exhibited desired porosity, hydrophilicity, tensile strength, rejection and long-term stability in salty environment under UV.	[32]
	1%		71		60							
	2%		61		82							
	3%		64		81							
TiO_2/PVP/PVDF/ NMP	0.5%			85	85		6.4 mg/L, 250 mL, rate 0.06 m/s (25 g/L NaCl)	UV-A 18 W, 6 h, 36 cm^2			Addition of pore-former PEG, increase the hydrophilicity and and hence improved water permeability and stability of PMs under salty water.	[23]
TiO_2/PVP/PEG/P VDF /NMP	0.5%	86	78	82	83	MB-water			97%	0.012		
						MB-NaCl						
HF (submersed)												
TiO_2/PVDF/DM Ac	3%	91	79			NP	100 mg/L, 7 L pH 6.8	UV-A 36 W, 4 h, 248 cm^2 (20 HF)	98% of R		7.5 wt% is the optimum TiO_2 content, and above this value decrease antifouling property, porosity and hence flux performance.	[26]
	7.5%		78						96% of R			
	10.5%		75						91% of R			
	15%		67						96% of R			

TiO_2 nanotube/ PVP/PVDF/NMP	0.1%	76	70		(POME)	TC = 742 mg/L, 15 L. pH 3	UV-A 8W, 4 h, 2.89 m^2	42.3%		The best flux, rejection and anti-fouling property observed for 0.5wt% TiO_2. High initial concentration decreases photoactivity of PMs, and alkaline condition improve flux.	[53]
	0.3%		65					57.1%			
	0.5%		64					67.3%			
	1%		61					50%			

Annex 5 Representative of Some Visible-light sensitive PMs used in different types of PMRs, their Photocatalytic Activity, and Other Performances of Membranes including Operating Conditions

Flat sheet or Hollow fiber membranes in Batch Process

PM type	wt% TiO_2 added	θ (°)		ε (%)		M	C_0 , V_0, pH, υ	I, t, A	D (%) or R (%)	k_{app} (min^{-1})	P (μg/(h ×cm^2))	Observation and other performances	Ref.
		Sup port	PM	Sup port	PM								
N-TiO_2/ PEG/PVDF/ DMAc (DLHF)	7.5%		70		35.1	BPA	5 mg/L	30W LED Visible light 6h	81.6%			N-doped TiO_2 DLHF shows the same photoactivity under UV and solar irradiation. 7.5 wt% is the optimum catalyst dose, above this content, properties improve but catalyst agglomerates due to higher surface tension between the solvent of dope solution.	[77]
	3%		82		9.6	RB5	5 mg/L		75% (for 7.5 wt% TiO_2)				[55]
	7.5%		70		35.1								
	10.5%		69		55.1								
Fe-TiO_2/ PEG/PSF/ DMAc & NMP (4:1)	0.05%					BPA	10 mg/L, 100 mL	500 W Xenon lamp, 3 h, 47.78 cm^2	90.8% (for 0.2 wt%)		6.33	Enhanced mechanical property and shows self-cleaning ability under visible-light. Optimum catalyst dose is 0.2 wt%. Higher inclusion of TiO_2 (0.25 wt%) decreases membrane mechanical stability.	[78]
	0.1%												
	0.15%												
	0.2%												
	0.25%												
N–TiO_2/ PMAA-*g*-PVDF/PAN/ DMAc	1%					Bentaz	10 mg/L, 100 mL. pH 7	UV 5063 lux, 3 h, 36 cm^2	42.9% for 3 wt% TiO_2		3.97	3 wt% catalyst dose optimum amount, above this value, roughness of the membrane surface increases because nanoparticles began to form lumps. Under basic conditions, positive charged bentazon adsorb more on PMs surface and enhance photodegradation.	[62]
	3%												
	5%							Sunlight 110000 lux, 3 h, 36 cm^2	99.8% for 3 wt% TiO_2		9.24		
Pd/N-TiO_2/ PSf/NMP	0.5%	79	66			EY	100 mg/L, 100 mL	450W Xenon lamp, 3 h, 9 cm^2	92.7%	0.0098	257.5	Improved hydrophilicity, porosity, visible light absorption and photoactivity but higher TiO_2 content increased membrane roughness due to embedded TiO_2 particle aggregation.	[61]
	1%		72						86.7%	0.0084	240.9		
	2%		73						97%	0.0149	269.4		
	4%		76						96.3%	0.0142	267.5		
	7%		77						97.3%	0.0169	270.3		
Flat sheet (Dead-end)													
Ag-TiO_2/ APTES/PVP /PVDF/DM Ac	0.1%	82	73			MB	3 mg/L, 30 mL. pH 7	Visible light, 1 h	80.3%			Smaller TiO_2 particles caused intracellular damage, and unique antibacterial performance. Meanwhile, Ag has inhibitory effect on the growth of bacteria; Thus these PMs shows excellent antibacterial activity towards E coli. Under visible light, provides a good self-cleaning ability and improved BSA rejection (from 63.43 to 89.80%)	[52]
	0.2%		68						86.7%				
	0.5%		61						90.1%				
Ag-TiO_2/ PVP/PVDF/ DMAc	0.01%	83	78			BSA		450 W Xenon lamp, 9 cm^2	97.21% of rejection, 8h				[59]
	0.03%		74										
	0.06%		57										

RGO-Ag-TiO_2/PEG/GLUT/CA	2.5 mg[†]		66		MB	20 mg/L	500 W Xenon lamp,	99% of rejection for all pollutant conditions			Inclusion of 10 mg of catalyst shows good and stable hydrophilicity and water permeability. Simultaneously degrade dye and separate oil–water emulsions under visible-light irradiation in a short time.	[58]
	5 mg		59		MB-oil							
	10 mg		43		RhB	30 mg/L						
	20 mg		37		RhB-oil							
mpg-C_3N_4/TiO_2/PVP/PSf/NMP	0.2%	71	66		SFMO	10 mg/L, 50ml	300 W Xenon lamp, 30 h, 8.5 cm^2	49%		0.96	Mechanically stable PMs prepared by adding nanoparticles. Increase hydrophilicity of the PMs, enhance water permeability albeit pore size decreased.	[60]
	1%		58					69%		1.35		
Flat sheet (Cross-flow)												
TiO_2/PVDF-TrFE/DMF	8%				Tartz	10 mg/L	Sunlight, 5 h, (38×12) cm^2 υ = 28 mL/s (for all C_0)	77.77	0.30		Increase in initial feed concentration (10-30 mg/L) reduced the photodegradation of tartzarine (78 to 47%). Meanwhile, increasing the feed flow rate (9.78-28 mL/s) enhance photodegradation efficiency (37-77%) due to larger turbulence from the higher flow rate, which promotes external mass transfer.	[33]
						20 mg/L		57.72	0.18			
						30 mg/L,		46.57	0.12			
3D-TiO_2/ZnO/PVDF (ALD)		95	40		MB	3.2 mg/L, 100 mL 300 mL	200 W Xenon lamp, 19.6 cm^2	95% (30 min)	0.11	31.02	Super-hydrophilicity of this visible-light active membrane shows enhanced anti-fouling performance.	[57]
					HA			73% (1 h)		35.75		
L–Histidine/TiO_2/CdS/PVP/PES/DMAc	0.1%	63	51		POME	1 g/L, pH 5.5, 150 L/h	500 W Halogen lamp,	100% (30 min)			Better performance observed after incorporation of 0.5 wt% catalyst, because above this load surface becomes rougher and nanoparticle agglomerates. Increase in initial feed concentration (1-5 g/L) reduced the permeation flux (31.4 to 11 $kg/m^2.h$). Meanwhile, increasing the feed flow rate (50, 150 L/h) also improved rejection efficiency and permeation flux. Due to turbulence as well as bigger Reynolds number from higher flow rate reduce the concentration polarization and membrane fouling.	[79]
	0.5%		47									
	1%		45									

[†] These amounts are deposited onto membrane grafting by PEG and GLUT through vacuum filtration method

[**] These are based on suspensions of TiO_2 on water and then membrane was immersed in this suspension to deposit TiO_2

Annex 6 Recipient to crystallize on-site synthesized TiO_2 nanoparticles on membrane

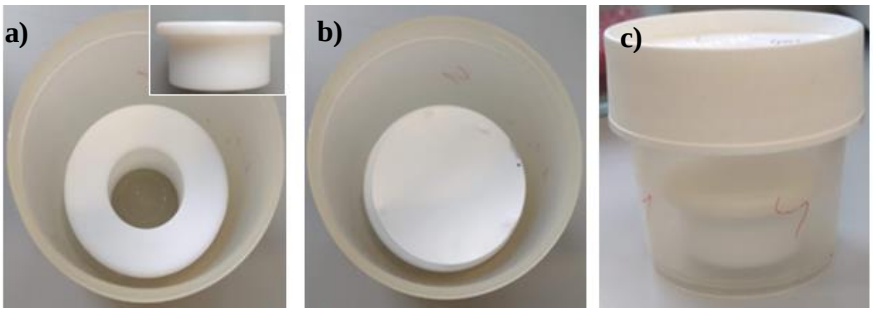

Annex 7 SEM images of the Membranes prepared from lower concentration (2 mM and 4 mM) sol-gel solution; a) Pure PVDF (0mM), b) 2mM, c) 4mM

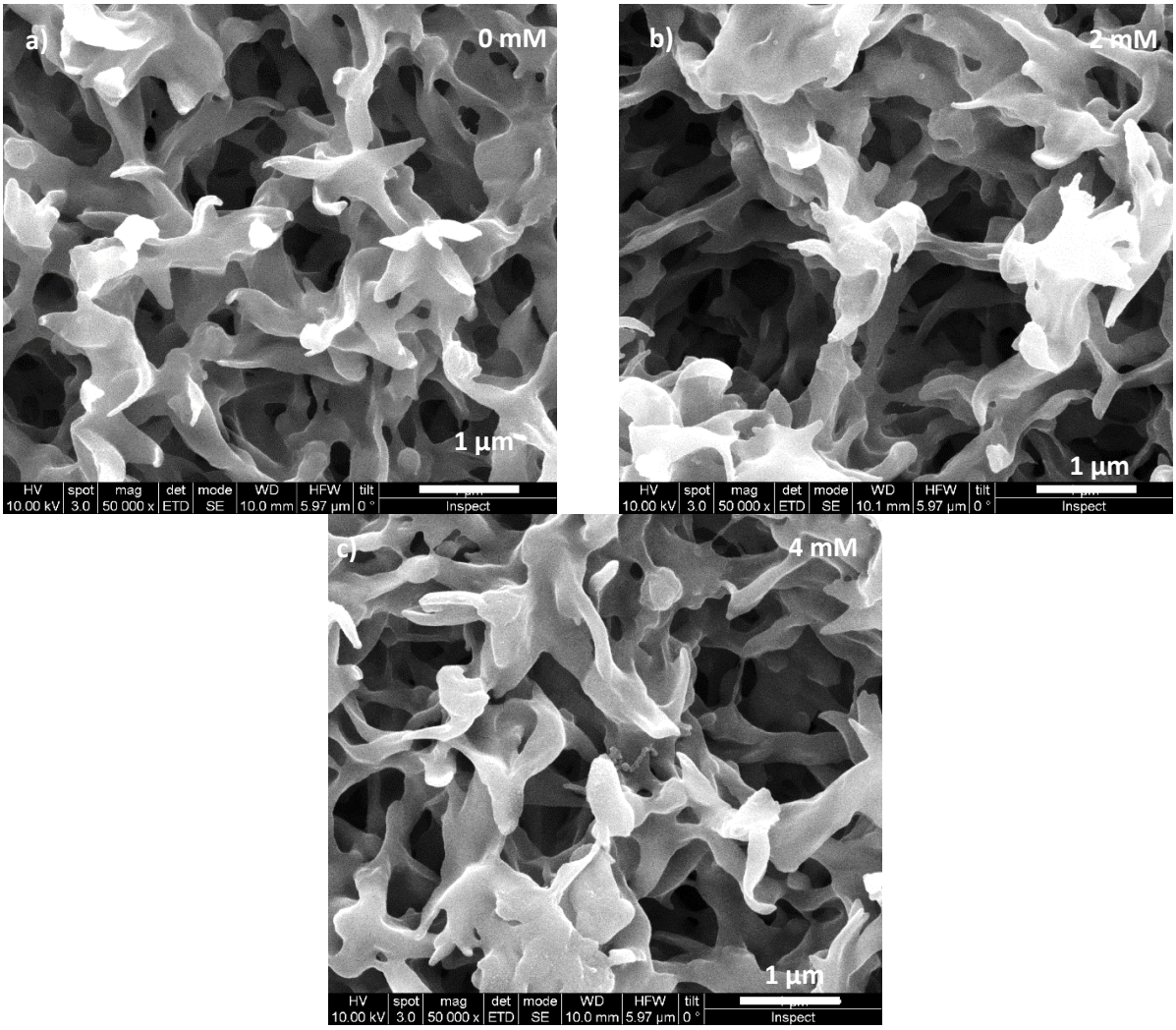

Annex 8 Histogram of the distribution of diameter of nanoparticles deposited on a) 8mM, b) 16mM, and c) 32mM

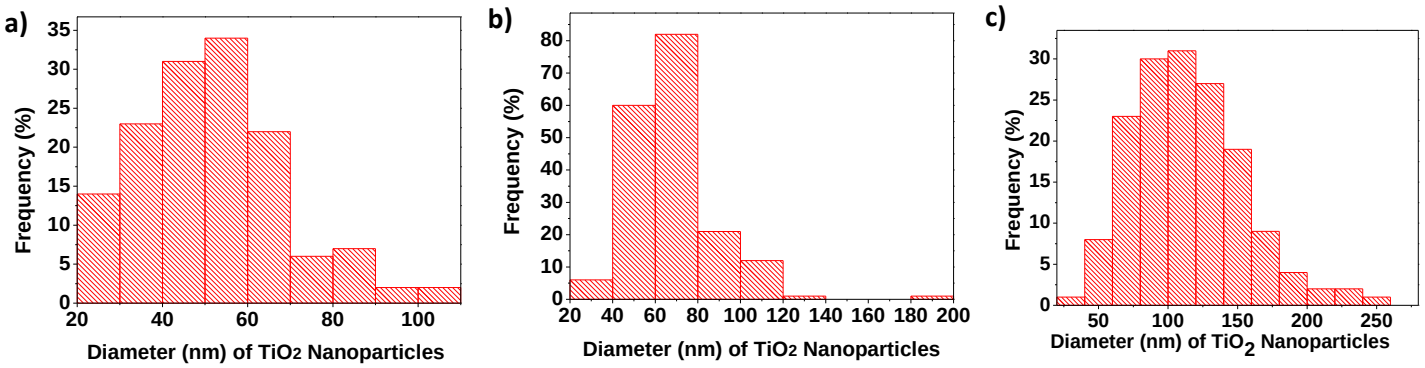

Annex 9 Effect of Mechanical Stirring on MB adsorption onto non-coated pure PVDF membrane a) adsorption at 200 rpm for 3 runs, b) adsorption at 300 rpm for 2 runs, c) adsorption at 400 rpm, and d) comparison of average adsorption rates for all runs.

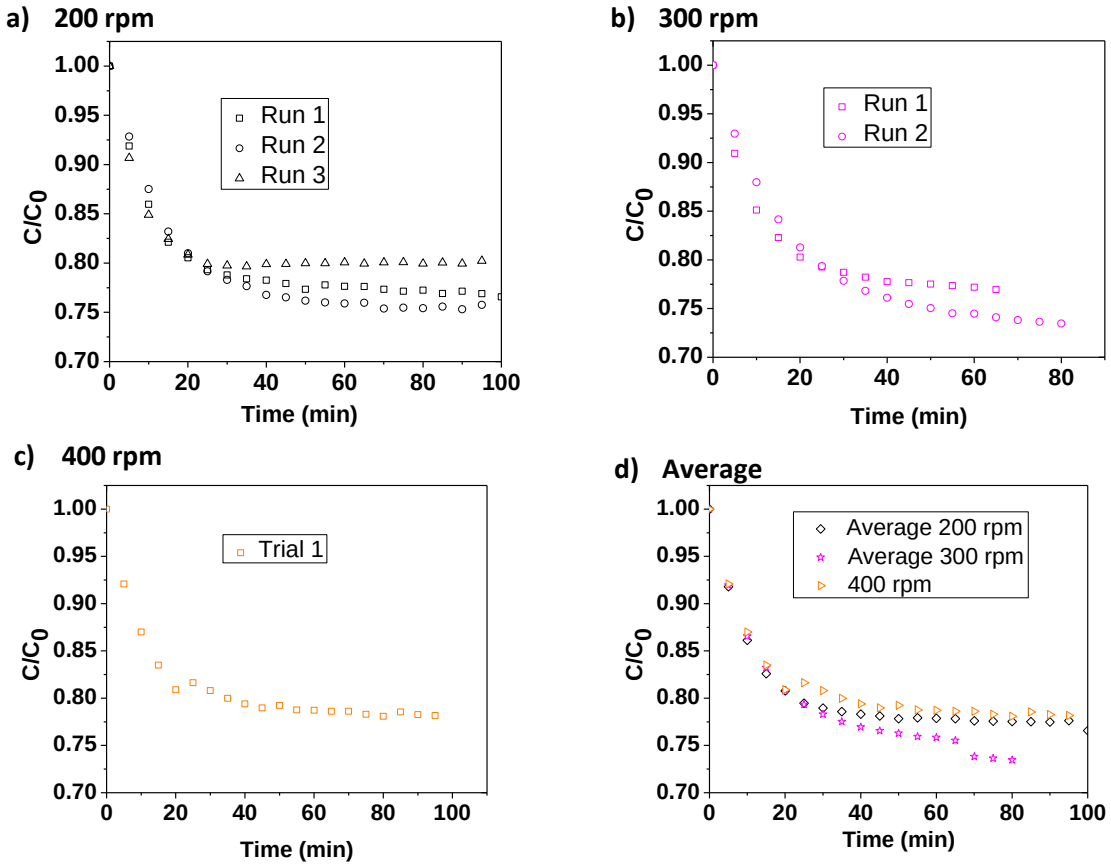

Annex 10 Histogram of the distribution of diameter of nanofibers of a) Electrospun pure PVDF, b) PPTM, and c) PTM